Comparison of a Land Surface Model (SSiB) to Three Parameterizations of Evapotranspiration—A Study Based on ISLSCP Initiative I Data

David M. Mocko* and Y. C. Sud

Laboratory for Atmospheres, NASA/Goddard Space Flight Center, Greenbelt Maryland

Received 22 May 1997; accepted 14 April 1998.

ABSTRACT: Four different methods of estimating land surface evapotranspiration are compared by forcing each scheme with near-surface atmospheric and soil- and vegetation-type forcing data available through International Satellite Land Surface Climatology Project Initiative I for a 2-yr period (1987–88). The three classical energy balance methods by Penman, by Priestley–Taylor, and by Thornthwaite are chosen; however, the Thornthwaite method is combined with a Mintz formulation of the relationship between actual and potential evapotranspiration. The fourth method uses the Simplified Simple Biosphere Model (SSiB), which is currently used in the climate version of the Goddard Earth Observing System II GCM. The goal of this study is to determine the benefit of using SSiB as opposed to one of the energy balance schemes for accurate simulation of surface fluxes and hydrology. Direct comparison of sensible and latent fluxes and ground temperature is not possible

* Corresponding author address: David M. Mocko, Code 913, Climate and Radiation Branch, Laboratory for Atmospheres, NASA/Goddard Space Flight Center, Greenbelt, MD 20771. Additional affiliation: General Sciences Corporation, Laurel, Maryland.

E-mail address: mocko@climate.gsfc.nasa.gov

because such datasets are not available. However, the schemes are intercompared. The Penman and Priestley–Taylor schemes produce higher evapotranspiration than SSiB, while the Mintz–Thornthwaite scheme produces lower evapotranspiration than SSiB. Comparisons of model-derived soil moisture with observations show SSiB performs well in Illinois but performs poorly in central Russia. This later problem has been identified to be emanating from errors in the calculation of snowmelt and its infiltration. Overall, runoff in the energy balance schemes show less of a seasonal cycle than does SSiB, partly because a larger contribution of snowmelt in SSiB goes directly into runoff. However, basin- and continental-scale runoff values from SSiB validate better with observations as compared to each of the three energy balance methods. This implies a better evapotranspiration and hydrologic cycle simulation by SSiB as compared to the energy balance methods.

KEYWORDS: Evapotranspiration; Soil moisture; Runoff and streamflow; Water/energy interactions; Frozen ground

1. Introduction

The Biosphere–Atmosphere Transfer Scheme of Dickinson et al. (Dickinson et al., 1986) and the Simple Biosphere Model (SiB) of Sellers et al. (Sellers et al., 1986) were the two landmark works that set the stage for more realistic parameterizations of the diurnal cycle of land surface fluxes and soil hydrology. Ever since, numerous other schemes have appeared in the literature. The Project for Intercomparison of Land-surface Parameterization Schemes experiment (Henderson-Sellers et al., 1993; Henderson-Sellers et al., 1995) compares the performance of these schemes under a variety of conditions. The Global Energy and Water Cycle Experiment's (GEWEX) Global Soil Wetness Project (GSWP) (International GEWEX Project Office, 1995) is a project for intercomparison of different land surface schemes being used in general circulation models (GCMs).

The bucket model of Manabe (Manabe, 1969) is the oldest method and has been extensively used in GCMs. The bucket uses a β as the ratio of actual to potential evapotranspiration, which is the evapotranspiration that would occur in the absence of water stress. The bucket had problems, however; some were due to its simple representation of vegetation and others were due to the definition of potential evapotranspiration itself. These problems have been discussed comprehensively in Sud and Fennessy (Sud and Fennessy, 1982) and Sud and Smith (Sud and Smith, 1984). Milly (Milly, 1992) established a connection between the bucket and the state-of-the-art biosphere models and, based on the complexity of the relation, concluded that it cannot be inferred that the bucket was inadequate as compared to the biosphere models. The bucket has also undergone improvements to generate subsaturated baseflow and is referred to as ''smart bucket'' or ''bucket with holes.''

Regardless of the above, the Climate and Radiation Branch at Goddard has its own history of developing simple models to arrive at soil moisture initialization. The bucket model was abundantly used for this purpose. Use of the Thornthwaite method for estimating evapotranspiration goes back to the works

of Mintz and Serafini (Mintz and Serafini, 1984; Mintz and Serafini, 1992), Serafini and Sud (Serafini and Sud, 1987), Mintz and Walker (Mintz and Walker, 1993), and Liston et al. (Liston et al., 1993). Most of these works, particularly the latest one, emphasized improving evapotranspiration by adding different physical effects to the existing schemes. The primary aim was to produce a realistic hydrology cycle and to generate soil moisture fields for GCMs.

Some studies focused on delineating the influence of SiB against a bucket (or slab) model in a GCM (e.g., Sud et al., 1990; Sato et al., 1989). These studies showed that SiB reduces evapotranspiration with huge differences in the circulation. Sud et al. (Sud et al., 1990) showed that the bucket produced excess evapotranspiration over vegetated land. Mintz and Walker (Mintz and Walker, 1993) were also confronted by the same problem with the Thornthwaite method; consequently, Mintz suggested an equation for the correction of the surface temperature as a function of soil moisture availability, which was designed to reduce the potential evapotranspiration. Liston et al. (Liston et al., 1993) used the Mintz–Thornthwaite method to produce soil moisture values to initialize Atmospheric Model Intercomparison Project (Gates, 1992; Lau et al., 1996) GCM integrations.

The current work is motivated by one fundamental question: how would different evapotranspiration schemes, using the same land–hydrologic model, affect the surface fluxes and land hydrology when driven by the same and most up-to-date $1^\circ \times 1^\circ$ resolution global data? Three of the four chosen methods use energy balance formulations. These consist of a version of the classic Penman (Penman, 1948) method (as discussed in Pan, 1990), the Priestley–Taylor (Priestley and Tayler, 1972) method, and the Thornthwaite (Thornthwaite, 1948) method in conjunction with a Mintz formulation for correcting potential evapotranspiration and β. The fourth method is the Simplified Simple Biosphere Model (SSiB; Xue et al., 1991). The goal is to quantify how much difference SSiB has made to the land scheme of GCMs that have been used for climate studies.

Section 2 contains a brief description of each of the four methods. In section 3, the datasets used as forcing and the model integration procedures are described. Section 4 contains derived values and fields, as well as comparisons to observational data. Section 5 has a summary and conclusions.

2. Description of the four schemes

The energy conservation equation at the Earth's surface is

$$R_{\text{net}} - G - M = \text{LE} + H, \tag{1}$$

where R_{net} (W m^{-2}) is the net radiation, G (W m^{-2}) is the ground heat flux, M (W m^{-2}) is the snowmelt heat flux (ignored in most conventional representations), and LE (W m^{-2}) and H (W m^{-2}) are the latent and sensible heat fluxes from the surface into the atmosphere. Under potential conditions (no soil moisture stress), LE and H are replaced by LE* and H*.

2.1. Energy balance methods

The integrations with the three energy balance (3EB) methods are performed with a daily time step because the 3EB methods have not been designed for periods

shorter than 1 day. There is also no explicit biosphere model, except for a semi-empirical relation between potential and actual evapotranspiration that varies from one method to the other. SSiB explicitly calculates a ground and a deep soil temperature (which can reduce or disallow water from draining or entering the soil depending on the soil temperatures), while the other methods do not. Otherwise, soil moisture exchange between three soil layers in the 3EB methods is identical to that in SSiB.

Here, R_{net} can be expressed as

$$R_{\text{net}} = (1 - \alpha)S_{\downarrow} + L_{\downarrow} - \sigma T_S^4, \tag{2}$$

where $S_{\downarrow}$ (W m^{-2}) is the incident shortwave radiation, α is the surface albedo, $L_{\downarrow}$ (W m^{-2}) is the incident longwave radiation, σ is the Stefan–Boltzmann constant, and T_S (K) is the surface temperature. Surface radiation data from International Satellite Land Surface Climatology Project (ISLSCP) Initiative I (IIIData; Sellers et al., 1996b) is used for the terms of incident shortwave and longwave. The input dataset provides 2-m air temperature T_A (K), which is used in place of T_S. Combining (1) and (2), the energy balance equation becomes

$$(1 - \alpha)S_{\downarrow} + L_{\downarrow} - \sigma T_A^4 = \text{LE} + H + G + M. \tag{3}$$

The ground heat flux in (3) is approximated following Jensen [Jensen, 1973, Eq. (3.19)]:

$$G = 48.45 \frac{(T_{m+1} - T_{m-1})}{\Delta t} \tag{4}$$

where T_{m+1} (K) is the mean T_A of the following month, T_{m-1} (K) is the mean T_A of the preceding month, and Δt is the number of days in the 2-month period.

The heat flux used for melting snow, M, in (3) is obtained from the snowmelt simulated by the SSiB integration, which has a rudimentary but physically based snowmelt parameterization. Statistics for grid points with snow cover provide a dataset of snowmelt rate as a function of 2-m air temperature, surface albedo, and sunlight hours of the day. Only grid points with more than 20 mm of water-equivalent snow depth were selected, and all those periods when either the snowmelt rate or the surface temperature was at or below zero were not considered. Snowmelt rate scatterplots were produced as a function of sunlight hours (h), surface albedo, and T_A (°C); inspection of data led to a proposal of a functional relation of the form

$$M = a + bT_A + c[h(1 - \alpha)]^3. \tag{5}$$

The best curve fit to this data yields $a = 7.95$, $b = 3.92$, and $c = 17.02$.

The energy balance methods relate LE to LE* by

$$\text{LE} = \beta\,\text{LE}^* \tag{6}$$

Here β varies from zero (no evapotranspiration) to one (potential evapotranspiration). After (6) is used to calculate LE, (3) is used to solve for the sensible heat H. The calculation of both LE* and β differ among the 3EB methods; the specific details are discussed below.

2.1.1. Penman method

Penman (Penman, 1948) combined the evaporation needed to transport water vapor in the boundary layer using an aerodynamics calculation between the surface and boundary layer with available energy constraints. With the effects of snowmelt energy, the resulting potential evapotranspiration is of the form [e.g., Mahrt and Ek, 1984; Pan, 1990, Eq. (4)]

$$\mathrm{LE}^* = \frac{(R_{\mathrm{net}} - G - M)\Delta + \mathrm{LE}_A}{1 + \Delta}, \tag{7}$$

$$\Delta = \frac{L}{c_p}\frac{dq_s}{dT}\bigg|_{T_A} = \frac{L}{c_p}\, q_s(T_A)\,\frac{b}{T_A^2}, \tag{8}$$

$$\mathrm{LE}_A = \rho_A L C_h V\,[q_s(T_A) - q_A], \tag{9}$$

where L is the latent heat of vaporization, c_p is the specific heat of dry air, b is 5417 K (from the Clausius–Clapeyron equation), $q_s\,(T_A)$ (kg kg^{-1}) is the saturation specific humidity at the 2-m air temperature T_A, q_A (kg kg^{-1}) is the 2-m air specific humidity, ρ_A (kg m^{-3}) is the density of the air calculated using the surface pressure p_A (hPa), C_h is the bulk aerodynamic vapor transport coefficient (or Stanton number), and V (m s^{-1}) is the 10-m wind speed. For the 3EB methods, C_hV is taken as the inverse of the aerodynamic resistance r_a (s m^{-1}).

For β, the precalculated curve fit relationship of Xue [Xue et al., 1991, Eq. (9)] is used. For vegetated land, β is a function of vegetation type and soil water stress, and is of the form

$$\beta = 1 - \exp\{-c_2[c_1 - \ln(W_2)]\}, \tag{10}$$

where c_1 and c_2 are vegetation-type dependent and represent the progression of closing stomata[1]. Values for c_1 and c_2 can be found in Xue et al. (Xue et al., 1991); however, the labels of c_1 and c_2 in this table were inadventantly reversed. The soil wetness of the root zone soil layer is W_2. For the case of bare soil, $\beta = W_1$, the soil wetness of the uppermost soil layer. Soil wetness is a dimensionless quantity varying from zero (dry) to one (saturated).

2.1.2. Priestley–Taylor method

Priestley and Taylor [Priestley and Taylor, 1972, Eq. (6)] give the Bowen ratio (the ratio of sensible to latent heat fluxes) under potential conditions as

$$\frac{H^*}{\mathrm{LE}^*} = \frac{s + \gamma}{as} - 1, \tag{11}$$

where $s = de_s/dT$ (hPa °C^{-1}) is the rate of change of saturation water vapor pressure with temperature taken at T_A [calculated using Brutsaert, 1982, Eqs. (3.24a) and (3.24b)], $\gamma = c_p p_A/0.622L$ (hPa °C^{-1}) is the psychrometric constant,

[1] Values for c_1 and c_2 can be found in Xue et al. (Xue et al., 1991); however, the labels of c_1 and c_2 in this table were inadvertantly reversed.

and a is an empirically determined scaling coefficient (see Mintz and Walker, 1993; Brutsaert, 1982); it is determined to be 1.27. Substituting the value of H^* from (11) into (1), and also allowing energy for snowmelt (M) as before, yields the Priestley–Taylor equation for potential evapotranspiration:

$$\mathrm{LE}^* = a(R_{\mathrm{net}} - G - M)\frac{s}{s + \gamma}. \tag{12}$$

The β used for the Priestley–Taylor method is the same as used for the Penman method.

2.1.3. Mintz–Thornthwaite method

Thornthwaite (Thornthwaite, 1948) related potential evapotranspiration to screen-level temperature and length of the day. The measurements were made over well-watered fields evaporating under near-potential conditions. The temperature measured, T_A^*, becomes the temperature of the air under potential conditions. To apply the method for all conditions, including deserts, T_A^* is computed from T_A and soil moisture availability β. Mintz and Walker [Mintz and Walker, 1993, Eq. (24)] approximated this value by (all temperatures in °C)

$$T_A^* = (0.83 + 0.17\beta)T_A. \tag{13}$$

The Thornthwaite equation for potential evapotranspiration as a function of T_A^* and h is

$$\mathrm{LE}^* = \begin{cases} 0 & T_{\mathrm{A}}^* \le 0°\mathrm{C} \\ \left[0.533\left(\dfrac{10T_{\mathrm{A}}^*}{I}\right)^a\right]\dfrac{h}{12} & 0 < T_{\mathrm{A}}^* \le 26.5°\mathrm{C}\ , \\ \left(-13.86 + 1.075T_{\mathrm{A}}^* - 0.0144T_{\mathrm{A}}^{*2}\right)\dfrac{h}{12} & T_{\mathrm{A}}^* > 26.5°\mathrm{C} \end{cases} \tag{14}$$

$$I = \sum_{1}^{12} i; \qquad i = (T_{\mathrm{m}}/5)^{1.514}; \qquad T_{\mathrm{m}} \ge 0°\mathrm{C}\ , \tag{15}$$

$$a = (6.75 \times 10^{-7}I^3) - (7.71 \times 10^{-5}I^2) + (1.79 \times 10^{-2}I) + 0.492. \tag{16}$$

For the Thornthwaite method, Mintz introduced a β function, defined as the ratio of the transpiration to the potential evapotranspiration minus the interception loss and soil evaporation; the relation was later adopted by Liston et al. (Liston et al., 1993). Then, β is assumed to be proportional to the inverse of the stomatal resistance r_s (s m^{-1}). Sellers (Sellers, 1985) wrote that it is inversely proportional to the ratio of the surface reflectances in the near-infrared and visible wavelengths. Finally, this ratio is related to the normalized vegetation index (NDVI) (Tucker et al., 1985), by

$$\beta = \frac{E_T}{E^* - E_{I,S}} \propto \frac{1}{r_{\mathrm{s}}} \propto \frac{I\eta_{(\mathrm{NIR})}}{I\eta_{(\mathrm{VIS})}} = \frac{(1 + \mathrm{NDVI})}{(1 - \mathrm{NDVI})} \tag{17}$$

From (17), β is solely a function of NDVI, which can be recast as

$$\beta = \gamma + \lambda \frac{(1 + \mathrm{NDVI})}{(1 - \mathrm{NDVI})}, \tag{18}$$

where γ is -0.45 and λ is 0.421. The NDVI data is from the IIIData and varies monthly. The maximum and minimum were chosen such that approximately 15% of all 14,637 points had NDVI at or outside the boundaries, depending on the season. The values of the constants are determined from a maximum NDVI of 0.55 and a minimum NDVI of 0.033 that correspond to potential and no evapotranspiration values.

2.2. Simplified Simple Biosphere Model (SSiB)

SSiB has been used as the land–atmosphere component of the Center for Land–Ocean–Atmosphere, Goddard Laboratory for Atmospheres, and, more recently, Goddard Earth Observing System I and II GCMs employed for climate work at the Climate and Radiation Branch. The prognostic variables are canopy temperature, soil surface temperature, deep soil temperature, water (or snow) on the canopy or ground, and soil moisture fraction for the three soil layers. The top two layers constitute the root zone, while the bottom (or recharge) layer can exchange moisture only via hydraulic diffusion and gravitational drainage. There is also a subsurface runoff following Liston et al. (Liston et al., 1993). Other processes in SSiB are the interception and evapotranspiration from vegetation leaves, influence of a stomatal resistance, and the partitioning of radiation into four components (direct and diffuse; infrared or visible).

3. Datasets, soil hydrology, and model integration

ISLSCP Initiative I data (Meeson et al., 1995) covers a 2-yr period, from 1 January 1987 to 31 December 1988. The horizontal grid spacing is 1° lat by 1° long. Permanent ice points are not analyzed, yielding a total of 14,637 time-varying soil moisture grid boxes. The temporal resolution of the data is either fixed, monthly, or six hourly. The fixed data include a land–sea mask, vegetation-type index, soil-type index, topographical slope, and total soil depth. A global distribution of vegetation types is shown in Figure 1. It should be noted that all C3 grassland is treated as C4 grassland in the current SSiB. Additional parameters are dependent on the soil or vegetation type. The values for these parameters can be found in Sellers et al. (Sellers et al., 1996a).

The monthly data include a roughness length, greenness factor, NDVI, leaf area index, fraction of photosynthetically active radiation absorbed by the vegetation canopy, snow-free and clear-sky albedo, displacement height, and bulk boundary layer and soil to canopy resistances. The values are linearly interpolated on a daily basis to vary steadily between the months. For the 3EB methods, the albedo used in (3) is a combination of the snow-free (based on NDVI data) and clear-sky (based on Earth Radiation Budget Experiment data) albedo. The clear-sky data is used as the surface albedo; however, the clear-sky albedo data does not extend over all grid boxes at all times. If the clear-sky albedo is missing, the snow-free albedo is used only if there was no snow on the ground. If there was snow on the ground, an albedo of 0.7 is used. The SSiB model uses the snow-

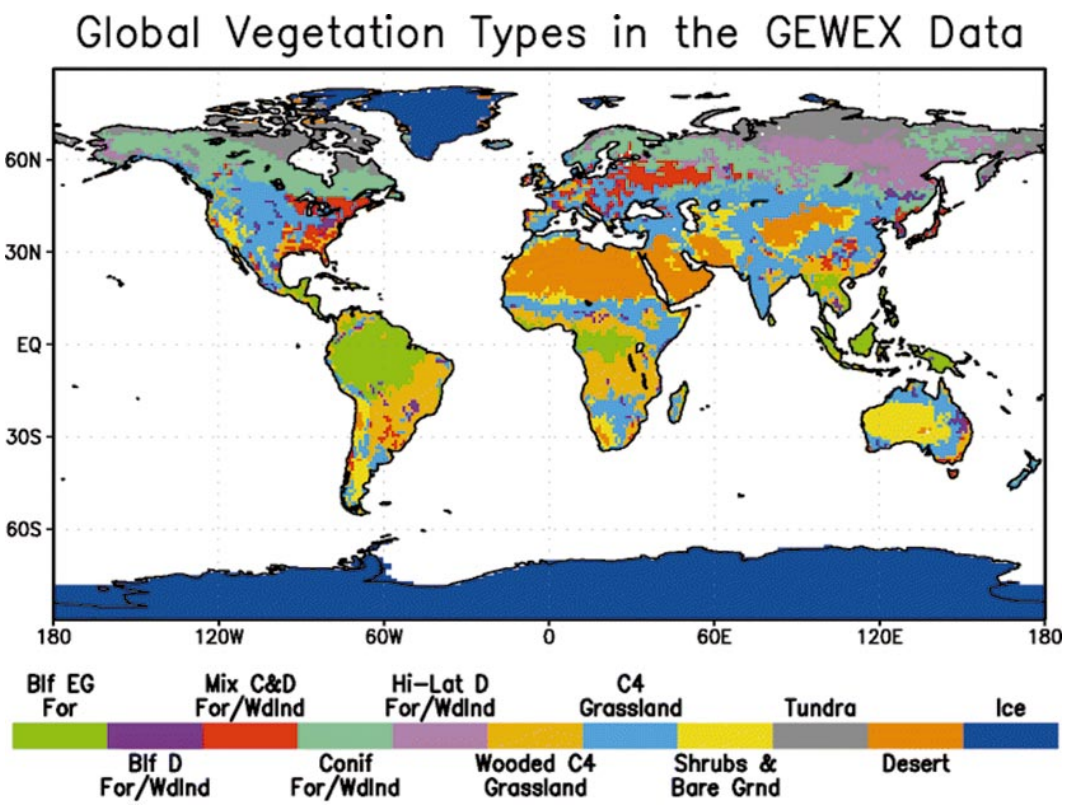

Figure 1. Vegetation type at each grid point used during model integration.

free albedo to produce a diurnal cycle of albedo over the four components, which is modified in the case of snow. For additional information, see Sellers et al. (Sellers et al., 1996a; Sellers et al., 1996c). As will be shown later, the final simulated albedo is very similar between the 3EB methods and SSiB.

The 6-h data consist of eight near-surface meteorological variables (temperature, pressure, humidity, wind speed, large-scale and convective precipitation, and long- and shortwave radiation), which provide the primary forcing for all four models. Each model is integrated independently of the others and no feedback of the fluxes is calculated into the near-surface variables. The SSiB model integration uses an hourly time step. The 6-h data is linearly interpolated to an hourly basis. The exception to this is the shortwave down data, $S_{\downarrow}$, which is interpolated using the cosine of the solar zenith angle to produce a realistic diurnal cycle. The 3EB methods use an integration with a daily time step, with the 6-h data averaged to a daily value.

All of the evapotranspiration parameterizations have the same hydraulic conduction process of water between layers as in SSiB. There are three soil levels with varying total depths from the IIIData. The top layer has a constant depth of 0.05 m for all grid points. Soil depth from the surface down to the bottom of the second layer is called the root zone depth and is generally around 1 m for veg-

etation types 6–11 and 1.5 m for vegetation types 1–5. There are six soil types that, together with the depths, are used to calculate the total capacity, wilting point, and field capacity value at each grid point. The wilting point (WP) in millimeters can be calculated by combining the Clapp and Hornberger (Clapp and Hornberger, 1978) soil moisture potential equation and the SSiB soil moisture deficit equation, as follows:

$$\mathrm{WP} = nD[-\exp(c_1)/\psi_s]^{-1/b}, \tag{19}$$

where n (dimensionless) is the soil porosity, D is the soil depth in millimeters being considered, ψ_s (m) is the matric potential at saturation, and b (dimensionless) is the slope of the retention curve on a logarithmic graph (also known as the Clapp and Hornberger parameter). The field capacity (FC) in millimeters is a function of soil type and can be determined either by saturating the soil in the model and allowing it to drain for several days or by integrating the soil moisture potential equation and assuming that the soil drains fully under the influence of gravity to give

$$\mathrm{FC} = nD\frac{(D_{\mathrm{total}} + \psi_s)^{-1/b+1} - (\psi_s)^{-1/b+1}}{(-1/b + 1)\psi_s^{-1/b}D_{\mathrm{total}}}, \tag{20}$$

where D_{total} (m) is the total soil depth. Table 1 lists the six soil types and the corresponding values of some soil-dependent variables. For the derivation of (20), see the appendix.

All three soil layers are initialized with 0.75 soil wetness. Using 1987 forcing conditions, each model is integrated from 1 January 1987 to 31 December 1987. The calculated soil wetness values (and soil temperatures and snow amounts, where applicable) at 31 December 1987 are then used again as initial conditions on 1 January 1987. The year 1987 is iterated 10 times for each parameterization or until the soil wetness values converge. The majority of points for the 3EB methods reach convergence quicker than SSiB. Points that take longer are located in cold and/or dry regions. After the 10-yr spinup, the resultant soil moistures are used as the initial conditions for the following 2-yr integration, 1987–88.

4. Integration results

4.1. Global values

Global averages for fluxes contributing to energy balance can be found in Table 2. The evapotranspiration from the Penman method (hereafter, PE) is the highest, while the Priestley–Taylor method (hereafter, PT) is nearly as high. Despite the same β formulation, the difference in the calculation of potential evapotranspiration has led to a difference of 4 W m^{-2} in evapotranspiration. The Mintz–Thornthwaite method (hereafter, MT) yields a lower global value for evapotranspiration. The unmodified Thornthwaite method [not shown, using β from Mintz and Walker, 1993, Eq. (7)] produces a much higher evapotranspiration, with values near PE and PT. The new equation for β for MT has greatly reduced evapotranspiration. The SSiB (hereafter, SS) value for evapotranspiration is between

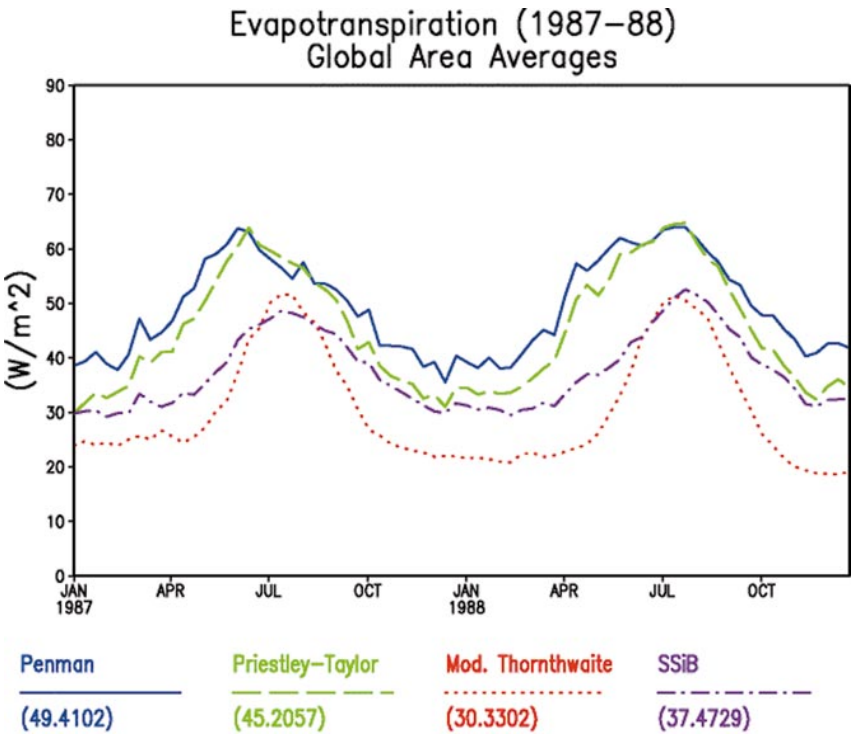

Figure 2. Time series of global area average of evapotranspiration of all four models.

these three methods, and was much closer to the other biospheric models participating in GSWP.

The time series of the global evapotranspiration is shown in Figure 2. Because the majority of land is in the Northern Hemisphere, the peaks of the curves occur in June–July–August (JJA), corresponding to a period of more solar energy, longer sunlight hours, and warmer temperatures. The PE method gives the highest values during nearly the entire period. The PT method gives similar values to PE during JJA but is slightly lower during December–January–February. The SS time series curve peaks slightly later into July than the other curves, and there is less of a seasonal cycle. The MT method has similar values of evapotranspiration during JJA, but is lower than the other methods during DJF.

The sensible heat values for 1987–88 are shown in Figure 3. The MT method yields the highest sensible heat, in keeping with the energy budget corresponding to low evapotranspiration. The two other energy balance methods, PE and PT, give slightly higher sensible heat values than SS, with the largest differences during JJA. Here again, the SS time series shows less of a seasonal cycle as compared to the 3EB methods.

The sum of the sensible and latent heat fluxes (evapotranspiration) from the 3EB methods is greater than the sum from corresponding values for the SS model. There are two reasons for this. One is that both the ground heat flux and snowmelt

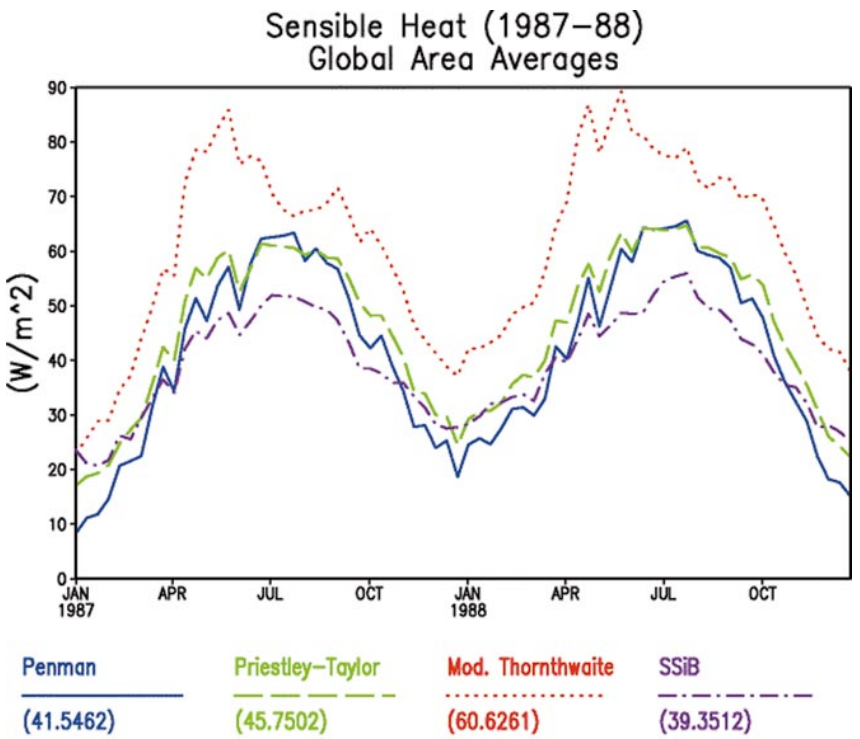

Figure 3. Time series of global area average of sensible heat of all four models.

heat flux (calculated explicitly by SS) are slightly greater than that of the 3EB methods. The second reason (presumably also the primary reason) is that the value of R_{net} from SS is lower than that of the remaining methods. As can be seen from Table 2, the net shortwave and incident longwave are identical (forcing data) between all four methods. The calculated longwave up is greater in SS by about 12 W m^{-2}; this corresponds to just over 2 K higher T_S for SS. The sensible heat flux is highly dependent on the difference between surface and screen-level air temperatures. Consequently, the lower value of emitted longwave in the 3EB methods has led to higher sensible heat flux without a significant change in the latent heat flux.

The surface outgoing longwave radiation (OLR) is lower in the 3EB methods because the observed 2-m air temperature T_A is used in place of T_S. The SSiB calculates a ground temperature; thus, its OLR value is higher. Although the daily time step has removed much of a potential source of error of OLR in the 3EB methods (owing to the diurnal cycle), it clearly has not eliminated it. Also, there is a problem in reporting values for sensible heat flux, which is heavily dependent on the difference between these two temperatures. For the purposes of this paper, it suggests that this problem would similarly happen in a land–atmosphere coupled model using energy balance. Because there is no feedback of the fluxes into the atmospheric conditions, any error in the calculated sensible heat flux is not

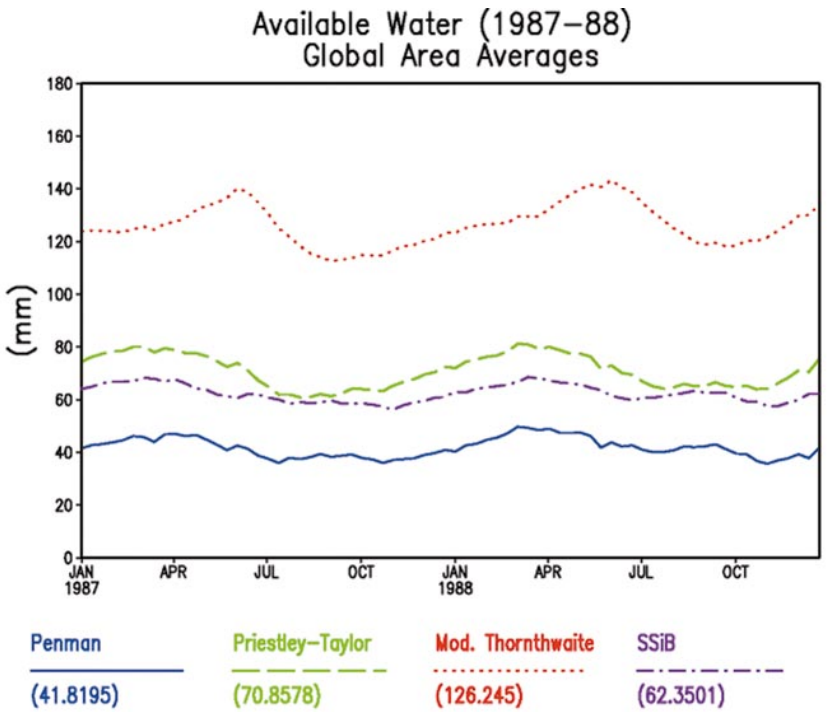

Figure 4. Time series of global area average of available water in top meter of soil of all four models.

considered significant. Likewise, surface temperature values in SS (not reported) do not have a feedback into these type of integrations.

Two-year values for the global available water are shown in Figure 4. The available water, expressed in millimeters, is defined as the soil moisture in the top meter of the soil minus the wilting point value; it shows PE has the driest top meter of soil with the highest evapotranspiration. The SS and PT methods have nearly the same amount of water in the soil, despite the latent heat flux being comparatively greater for PT. The MT method, with the lowest evapotranspiration, has produced the wettest top meter of soil.

The PE method gives the lowest value of runoff among the four (Figure 5). High evapotranspiration has greatly dried the soil and reduced the runoff. The PT method gives slightly higher runoff as compared to PE; however, it is less than that of SS. In fact, SS produces a sharper seasonal cycle in the runoff, with a May to July ''high water'' mark as a result of snowmelt and increase of convective precipitation over a larger percentage of land area. The MT method produces high runoff during DJF, as many grid points have nearly saturated soil.

A global distribution of the 2-yr annual average of evapotranspiration can be seen in Figure 6a and Figure 6b. Values in the Tropics for PE are generally 4–6 mm day^{-1}, with peaks above 6 mm day^{-1} in the Amazon and major islands. The PT values are generally similar, although its peaks are below 6 mm day^{-1}.

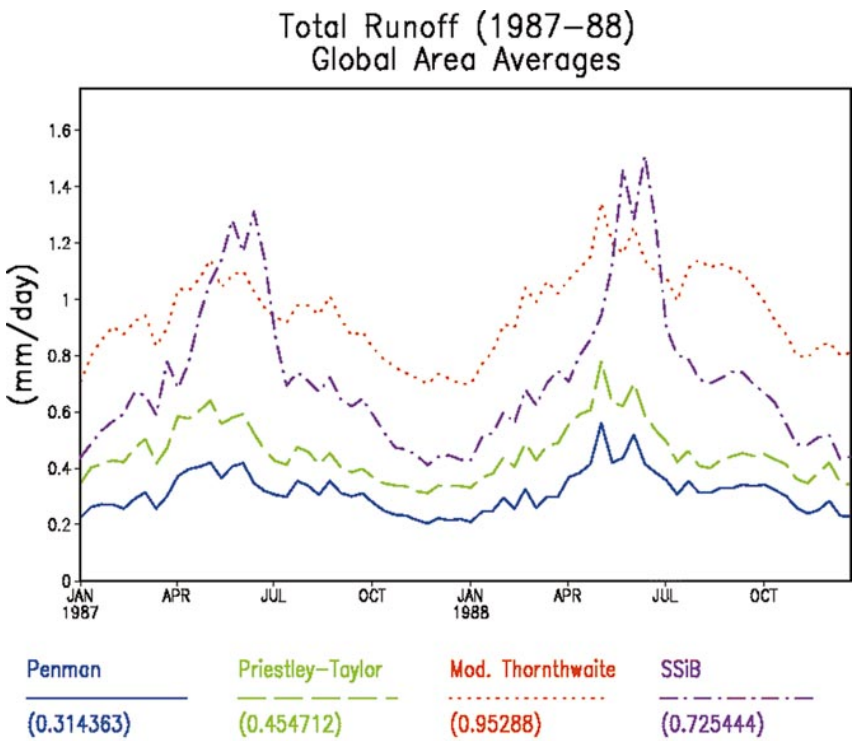

Figure 5. Time series of global area average of total runoff of all four models.

Evapotranspiration is lower with MT, particularly the area of below 0.25 mm day^{-1} has broadened while tropical values remain below 4 mm day^{-1}. For SS, a larger area contains average values of between 2 and 4 mm day^{-1}, and there is very small evapotranspiration at extreme high latitudes.

Datasets from the SS integration are available online from the Goddard Climate and Radiation Branch's http://climate.gsfc.nasa.gov/eoshpc/EOS HPC.html

4.2. Vegetation-type dependent values

It can be instructive to separate some model output variables by vegetation type and compare them among the methods. This type of comparison can offer insight into the nature of differences between the 3EB methods and the biospheric influences such as invoked in SS. Table 3 shows how the input precipitation, temperature, and radiation varies between vegetation types for the 2-yr global average. Description of each vegetation type with index number can be found in Xue et al. (Xue et al., 1991).

The evapotranspiration as a function of vegetation type can be found in Table 4. Generally, PE gives the highest evapotranspiration for each vegetation type, PT the next highest, then SS, and MT gives the lowest. The precipitation has the strongest effect on the magnitude of evapotranspiration. Types 4, 5, and 10 have below-zero average 2-m air temperatures, but warm temperatures, long sunlight

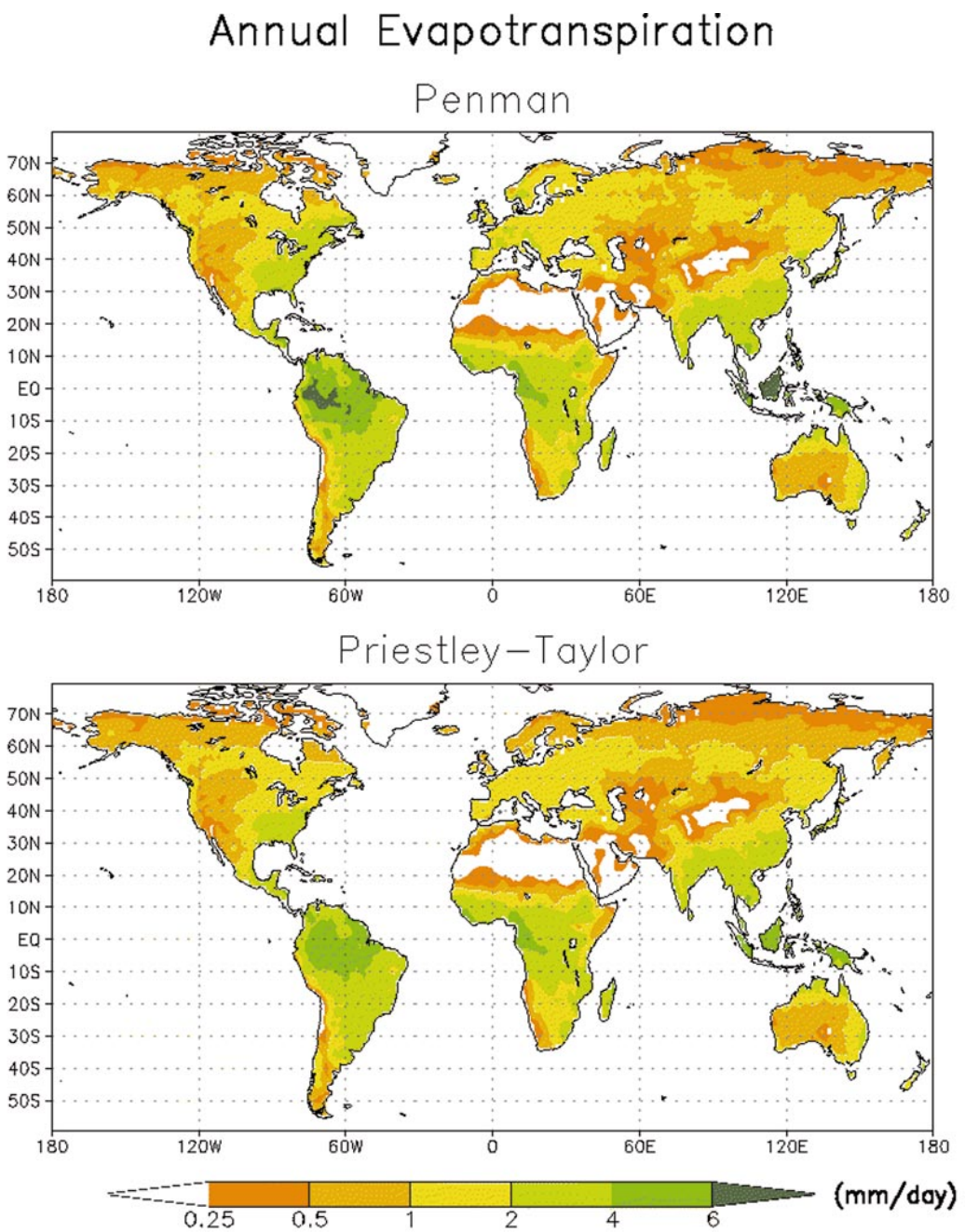

Figure 6a. Two-year annual average of evapotranspiration for PE (top) and PT (bottom).

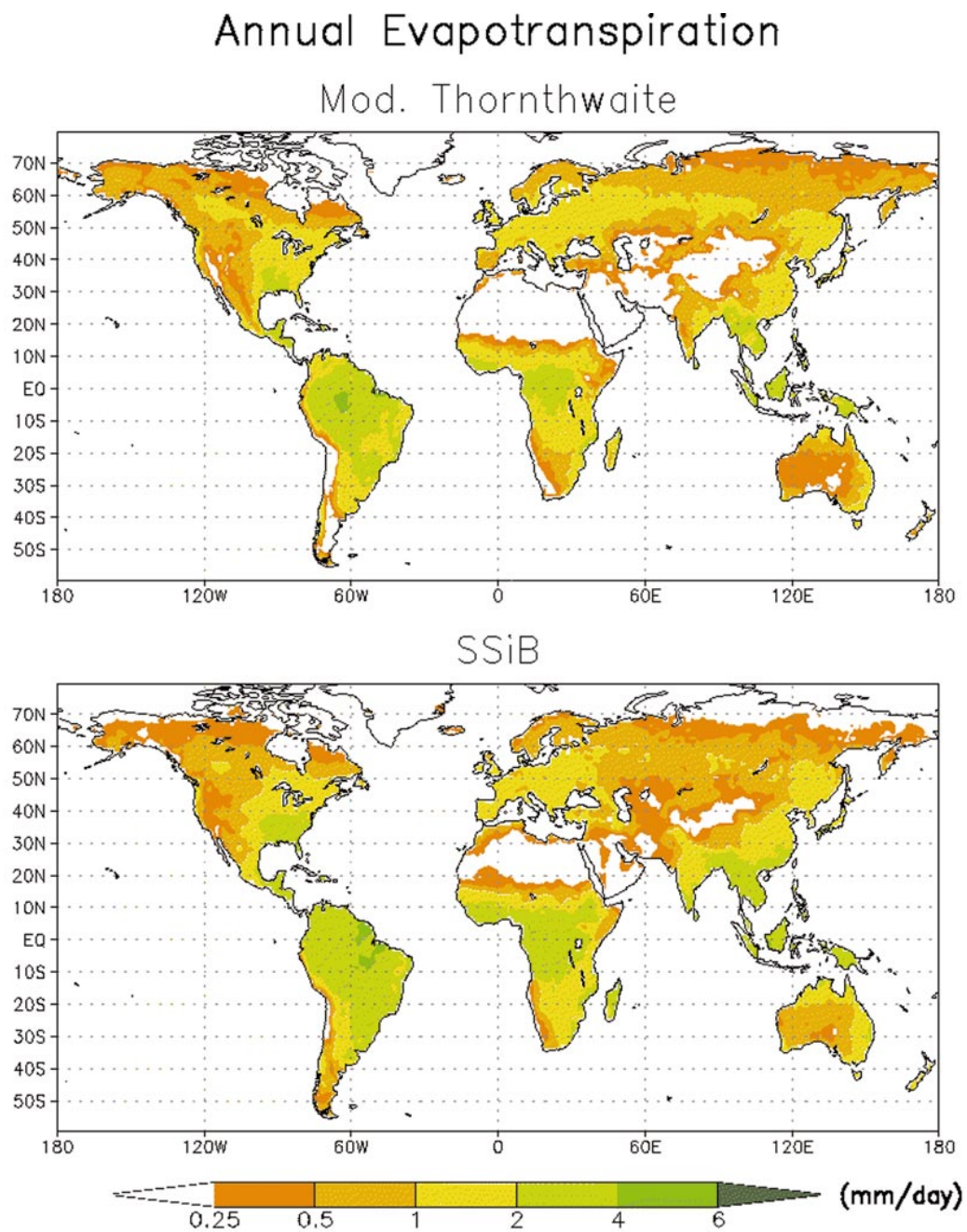

Figure 6b. Two-year annual average of evapotranspiration for MT (top) and SSiB (bottom).

hours, and available water from spring snowmelt provide high evapotranspiration amounts during the summer season.

The evapotranspiration is generally twice as large in vegetation type 1 as in type 2. The average precipitation over type 1 is similarly about twice that over type 2, while the shortwave down is about the same. The PE and PT methods give much higher evapotranspiration over type 1 than does SS. For these two methods, differences over tropical regions are larger than for other vegetation types, while the evapotranspiration is at or near the potential rate. The SS method has lower evapotranspiration because the biosphere model uses stomatal resistance for vegetation. This stomatal control shuts off evapotranspiration at night, and for very dry conditions, as well as for cold or very warm conditions.

Over regions with less vegetation and low precipitation (types 7, 9, 10, 11), all four methods give similar evapotranspiration. The MT method gives higher values than SS for types 4, 5, and 10, where the summer evapotranspiration rate may be too high. In other regions, the MT evapotranspiration is too low. This may be the outcome of the NDVI maximum and minimum chosen for the calculation of β and/or the zero evapotranspiration produced during the winter.

The average available water for each model aggregated by vegetation type can be found in Table 5. The PE method gives the driest soil for nearly all types. The MT method has much wetter soil than the other three for types 7, 9, and 11. In these subtropical to temperate regions, the evapotranspiration is nearly zero during the winter, and the soil moisture remains wet all winter long. The PT method has wetter soil than PE and SS for types 1, 3, 4, and 5.

The runoff for each model aggregated by vegetation type can be found in Table 6. The MT method generally gives the highest runoff. However, vegetation types 1, 6, 9, and 11 give much higher runoff for MT than the others. The higher values of 2-m air temperatures in these regions have caused a high potential evapotranspiration. However, the β may be too low for these vegetation types; therefore, the soil stays wet and runoff increases. The PE and PT methods give low runoff for most vegetation types, but PT is larger for types 1, 3, and 4. For these three types where PT also gives lower evapotranspiration and wetter soil than PE. The SS runoff has high runoff in types 4 and 10, which are areas with significant snowmelt.

4.3. Regional comparisons

The time evolution of land hydrology and surface fluxes in specific regions on the Earth is viewed through time–longitude transects. For these plots, the ordinate is a line across several longitude bands at a fixed latitude. The abscissa is time from January 1987 to December 1988. The first such transect is across 38°N within the United States, from 120° to 80°W. Figure 7 shows the observed precipitation in this area during this time. The evapotranspiration, precipitation minus evapotranspiration, and available water as determined by PE can be seen in Figure 8. The soil remains generally dry (less than 20 mm available water) except east of 95°W from November to April. The evapotranspiration is slightly reduced in the winter and is at its highest following precipitation events during the summer. The PT transect (Figure 9) shows a stronger seasonal cycle in evapotranspiration,

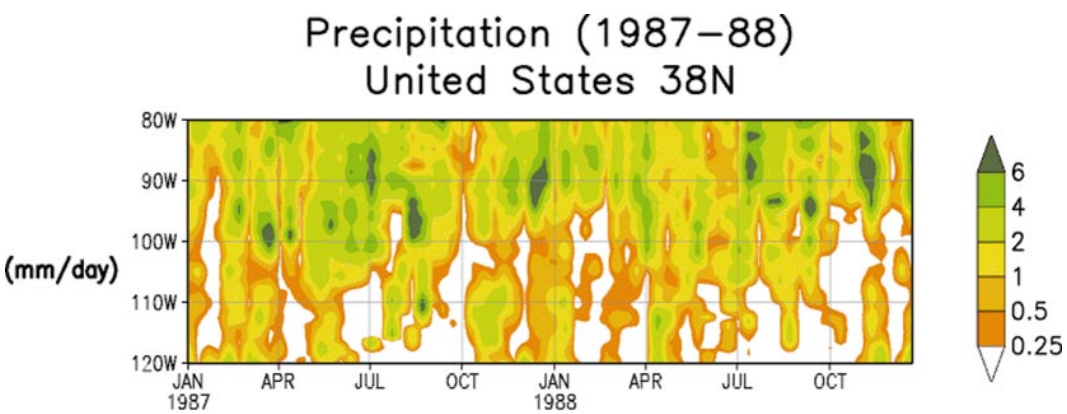

Figure 7. Time–longitude transect of precipitation for the United States across 38°N.

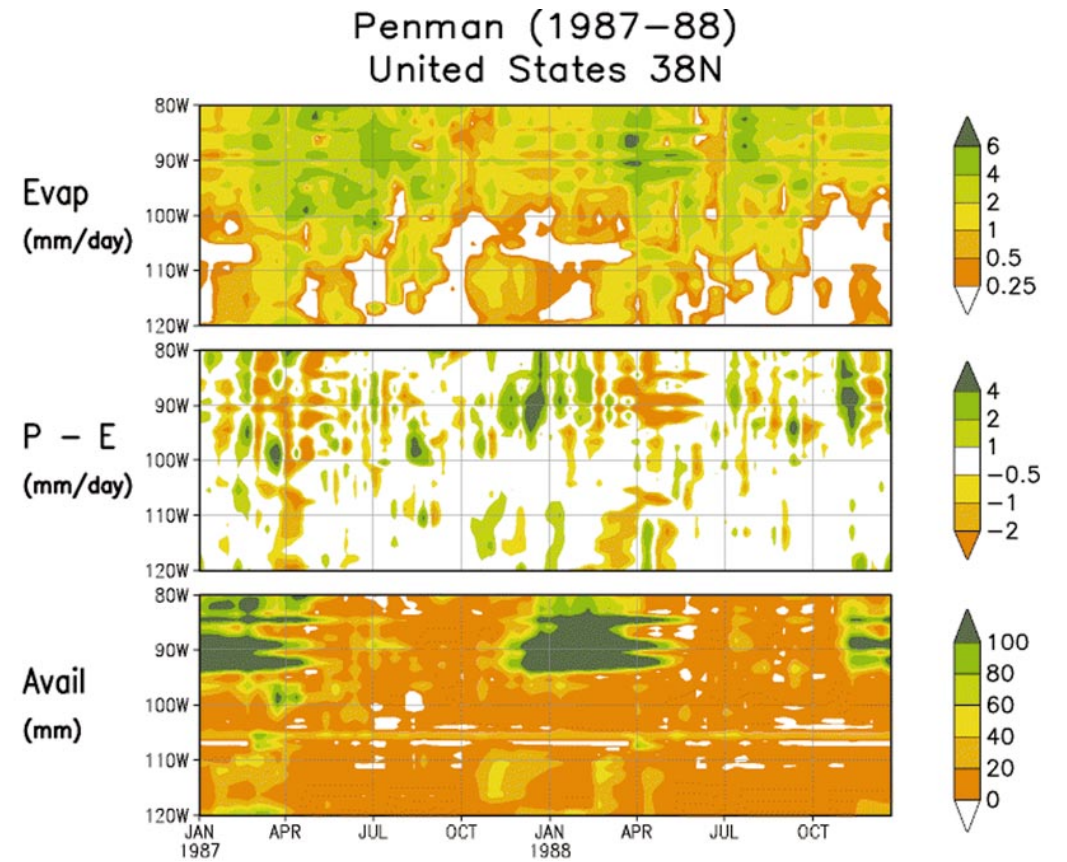

Figure 8. Time–longitude transect of evapotranspiration (top), precipitation−evapotranspiration (middle), and available water (bottom) for the United States across 38°N for PE.

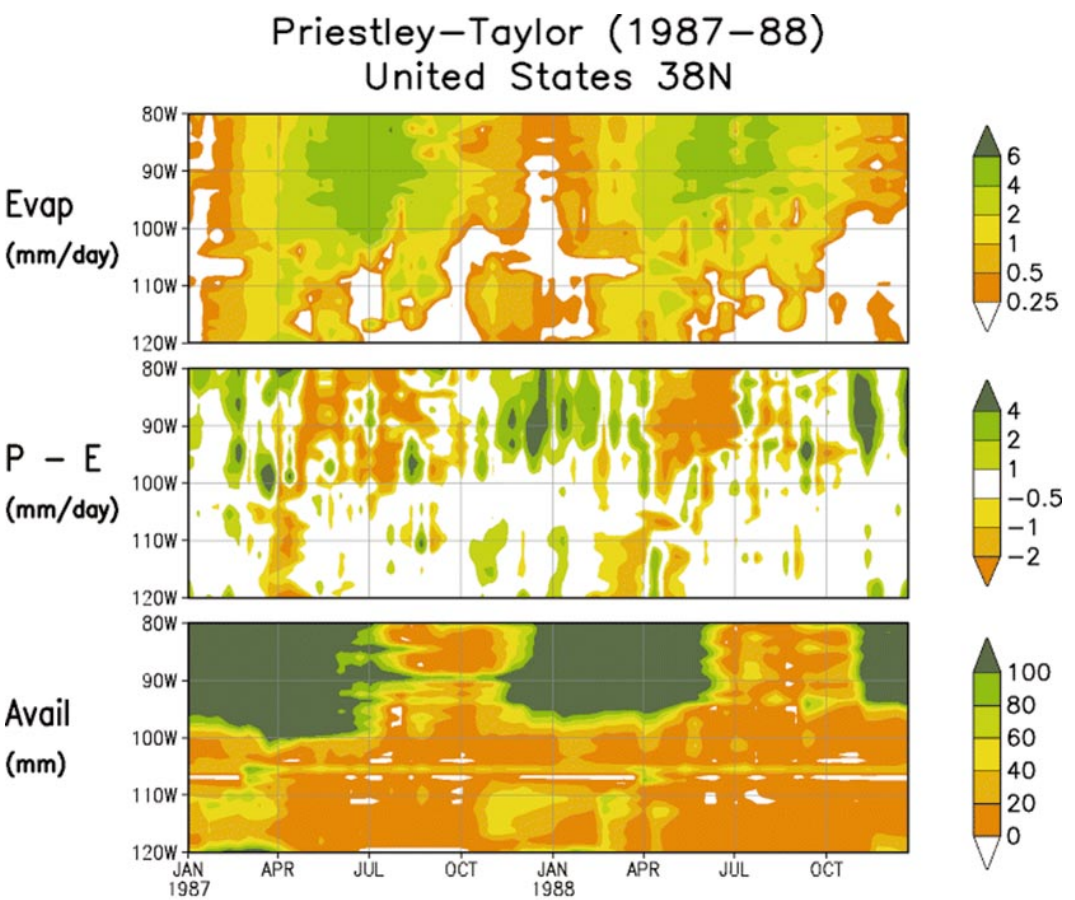

Figure 9. Same as Figure 8, but for PT.

which also results in more pronounced episodes of $P-E$ differences. Wet soil conditions now reach near 100°W and begin earlier in the winter. Also found is drier soil between 90° and 100°W during 1988 than during 1987, corresponding to a drought observed in the central United States at this time. The MT transect (Figure 10) gives a strong seasonal cycle in evapotranspiration, with very small or zero values given during a long time stretch in winter. The soil is very wet at nearly all longitudes. The SS transect (Figure 11) of evapotranspiration shows a clear annual cycle. The available water is zero or below zero west of 100°W. A negative value occurs when the moisture in the top meter of soil has fallen below the wilting point as given in (19). The wilting point, although the same in each of the four methods, could be too high as a result of the coefficients and soil–vegetation types used in its calculation. The dry soil conditions for the drought in 1988 is captured west of 95°W from April to September better in SS than in any of the 3EB methods.

Another set of transects examined is in northwest Russia at 57°N from 25° to 60°E. Figure 12 shows the precipitation in this area for 1987–88. There is not

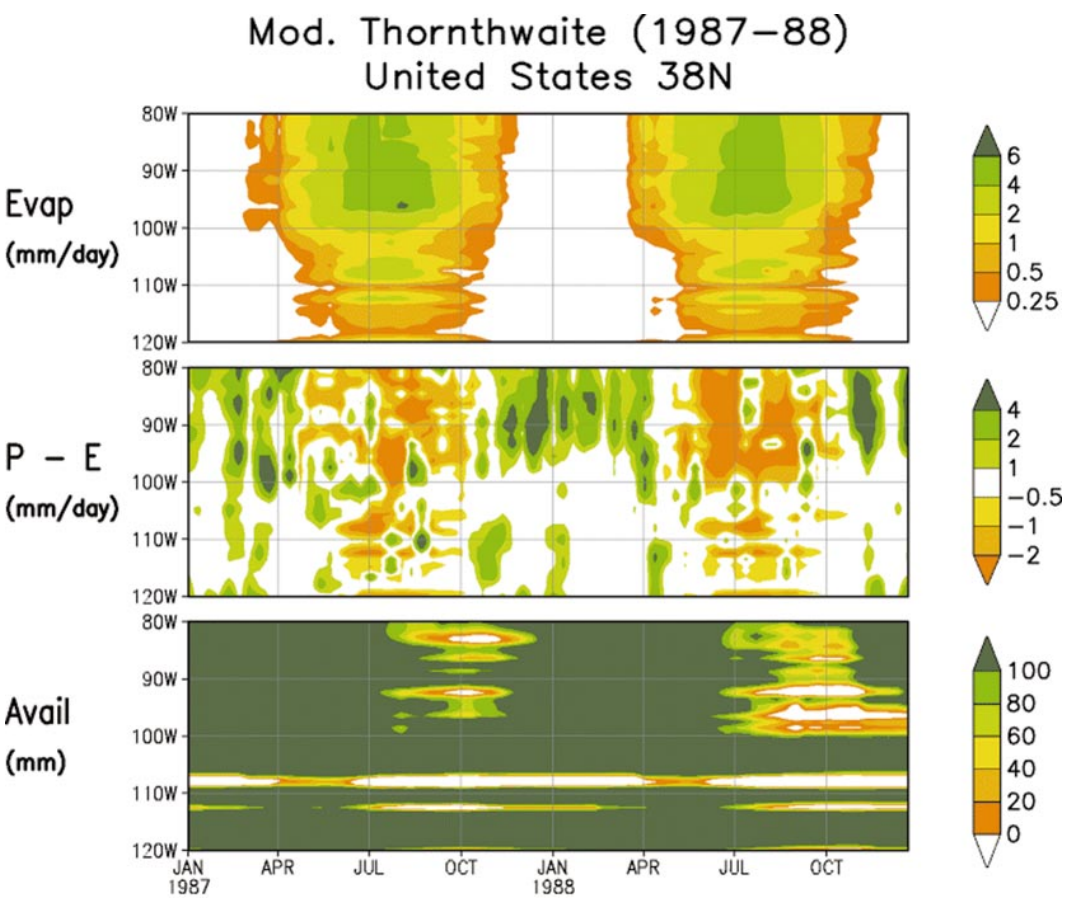

Figure 10. Same as Figure 8, but for MT.

much of a seasonal cycle, although winter is dominated by snowfall. Figure 13 is the PE transect, which shows the evapotranspiration has a strong seasonal cycle and is nearly zero between November to April. At this time, R_{net} is very small and the potential evapotranspiration is correspondingly small. Short-lived peaks of evapotranspiration and runoff occur in May after snowmelt leads to an increase of water infiltration. The PT transect (Figure 14) shows the evapotranspiration is again highly seasonal, but the magnitudes are slightly lower and shorter lived than from PE. The soil becomes much wetter in this area. The convergence reached after the 10-yr spinup cycle yields a wetter soil from the shorter and lower period of evapotranspiration. The MT transect (Figure 15) gives a shorter summer period of evapotranspiration than the previous two methods, although the peak values are higher. The potential evapotranspiration for this method depends on the sunlight hours and surface temperature. Again, the soil has remained wet at nearly all locations. The SS transect (Figure 16) has evapotranspiration continuing later into the winter than previous methods. There is a strong east to

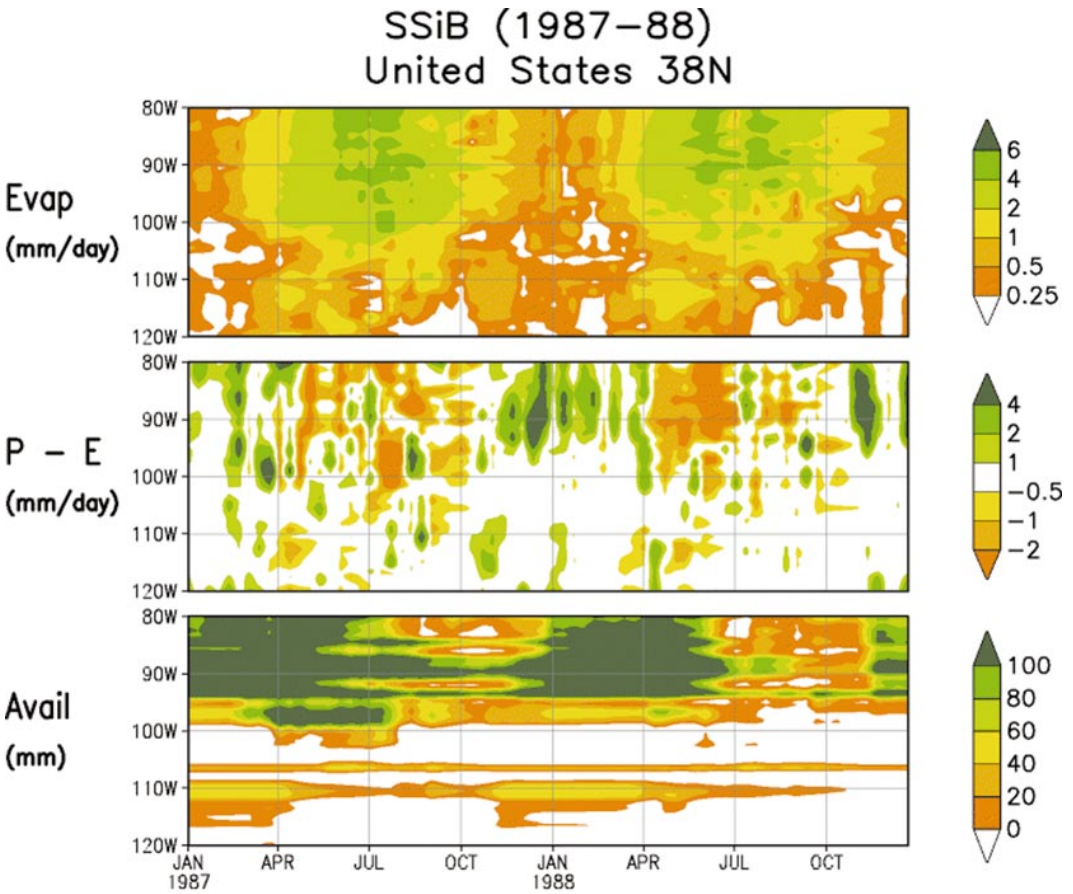

Figure 11. Same as Figure 8, but for SSiB.

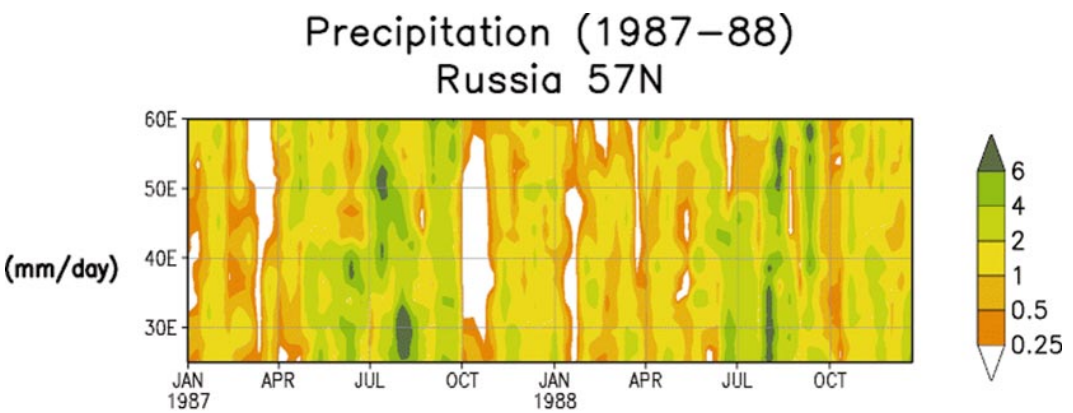

Figure 12. Time–longitude transect of precipitation for Russia across 57°N.

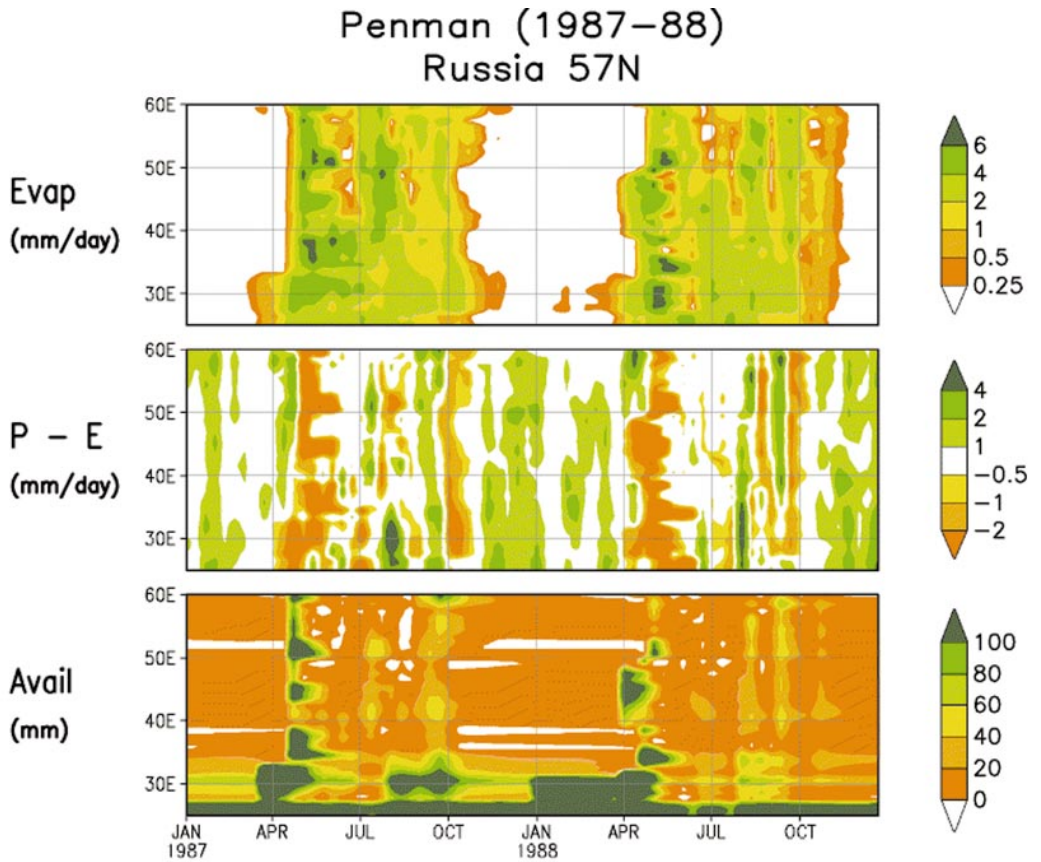

Figure 13. Time–longitude transect of evapotranspiration (top), precipitation−evapotranspiration (middle), and available water (bottom) for Russiaacross 57°N for PE.

west gradient across 40°E in the amount of available water. This gradient is likely in response to changing soil and/or vegetation types.

Other areas examined in this method include the Sahel and the Amazon (not shown). While results from the Sahel are generally similar, the PE and PT methods produced higher evapotranspiration in the rainy season in the Amazon than SS, while MT was generally lower. The effect of the biospheric control in SS in reducing evapotranspiration is again found.

4.4. Validation against observations

Accurate data for global land values of energy fluxes are not available. Comparisons that can be made, however, are of runoff and soil moisture values produced by the method to that measured.

4.4.1. Soil moisture

Global soil moisture values are not available. There are regional observations, however. For the time period of 1987–88, two such regions are examined in this

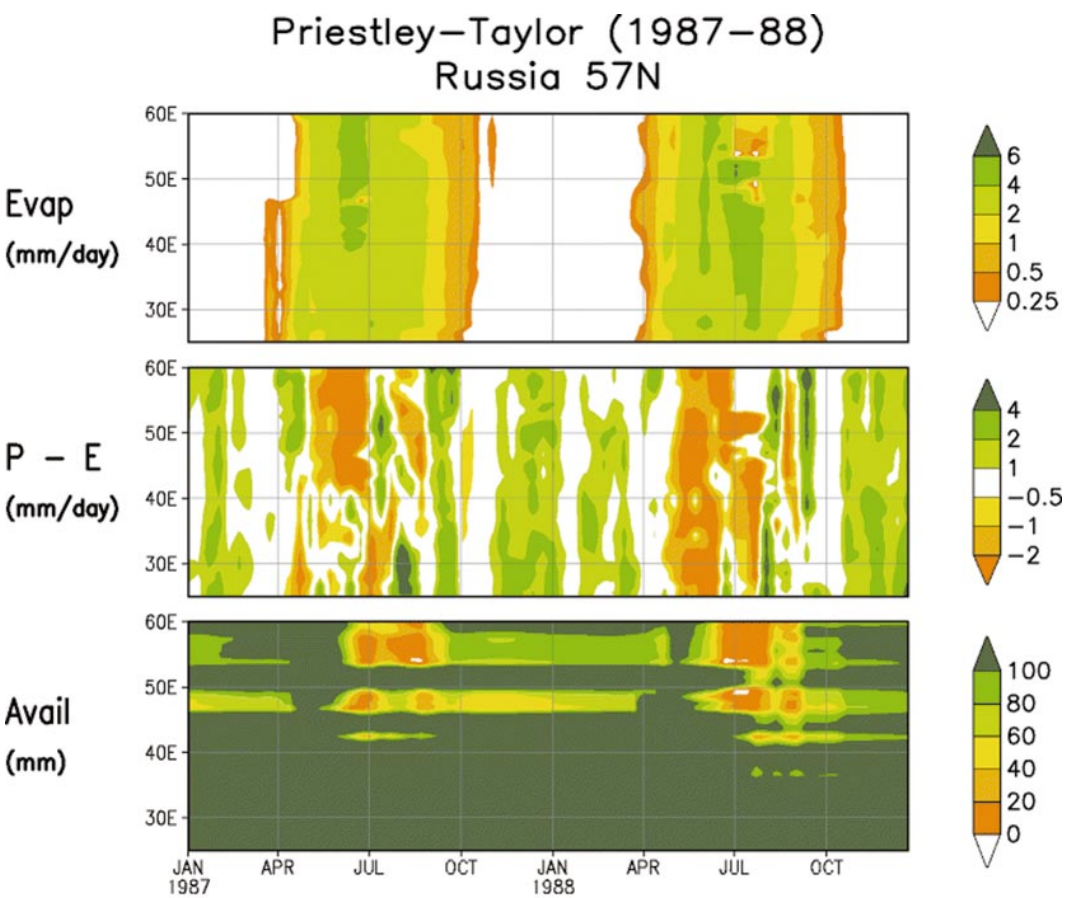

Figure 14. Same as Figure 13, but for PT.

study; one in northwestern Russia and one in the central United States across the state of Illinois. All soil moisture values in this section refer to available water in the top meter of soil.

Russian data was collected over agricultural fields during the growing period (10 April to 31 October). The fields carry winter and spring wheat crops. This data is based on 500 agrometeorological stations, as detailed by Vinnikov and Yeserkepova (Vinnikov and Yeserkepova, 1991). The soil moisture values were averaged from 55° to 65°N and from 20° to 60°E. This area includes the Russian transects previously examined. Observations are separately aggregated for winter and summer wheat crops. A second averaging region is within the state of Illinois, 38° to 42°N and 88° to 90°W, and is located in the north-central United States. This area is very near the U.S. transects. This dataset contains weekly data for the growing season and monthly data for the winter season. The region is almost entirely composed of cultivated agricultural fields, as detailed by Hollinger and Isard (Hollinger and Isard, 1994).

Figure 17 shows the time series of the available water in the top meter of

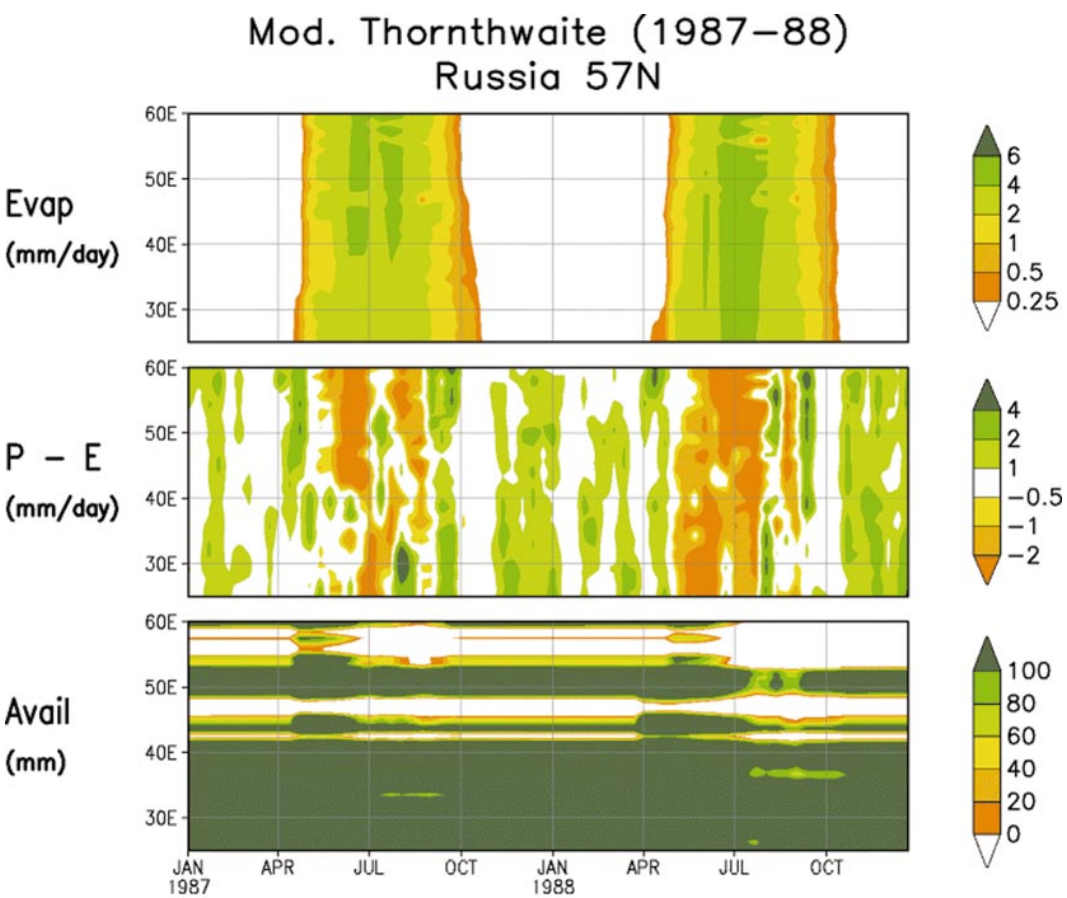

Figure 15. Same as Figure 13, but for MT.

soil for the observations and for all four methods for both the Russian region and the Illinois region from 1 January 1987 to 31 December 1988. As expected, PE, which consistently gives the highest evapotranspiration, gives the lowest available water. In Russia, PT and MT provide similar available water values in the summer to the observations. However, SS is excessively dry, especially during and immediately after a period of strong snowmelt. On the other hand, in Illinois, SS does much better, capturing the annual cycle of available water. The summer of 1988 was a drought year in this region, and SS gives lower available water at this time similar to the observations. Again, PE has soil that is too dry, especially in the spring and summer. The MT method has soil that remains wet during the spring and summer, most likely from a reduced evapotranspiration. The PT method gives available water similar to SS, only drier in the summer and wetter in the winter.

These two plots represent results at only two specific regions. Any conclusions drawn may change from region to region. It appears, however, that problems

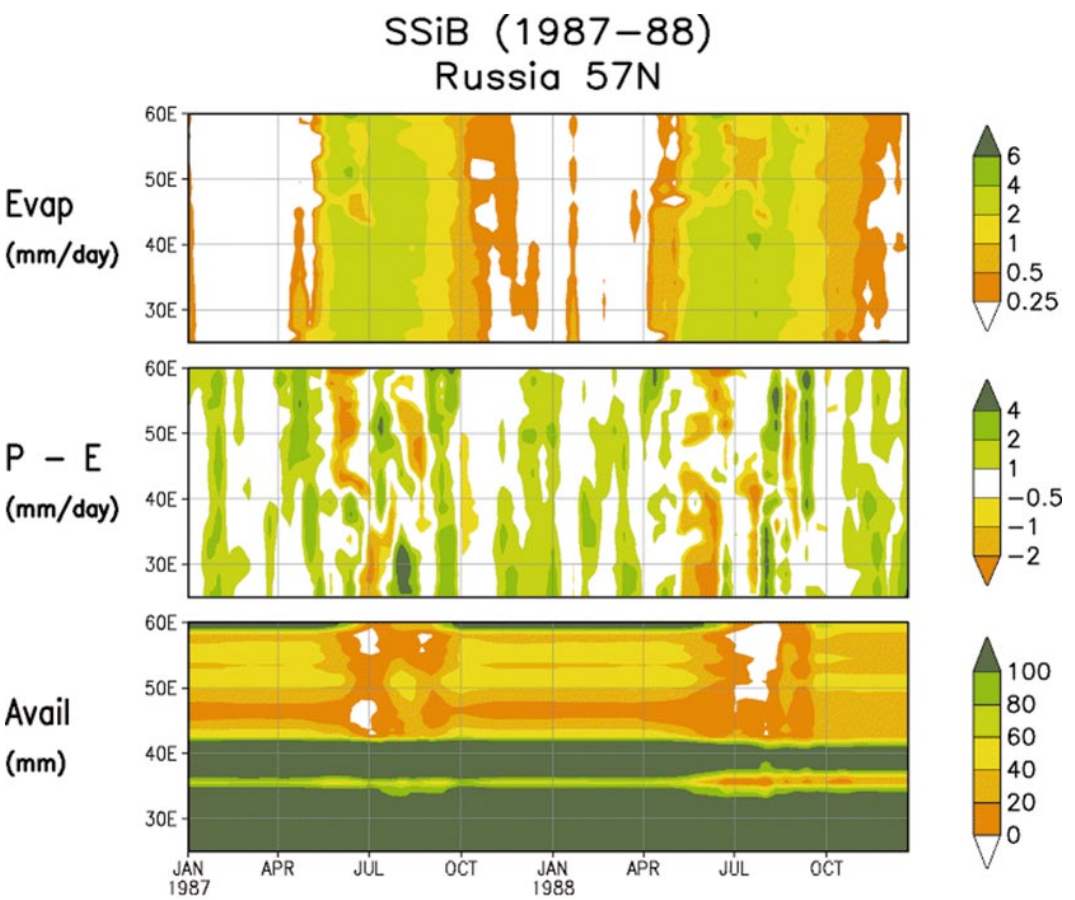

Figure 16. Same as Figure 13, but for SSiB.

in SS are related, in large part, to the handling of snowmelt over land that is in the process of freezing or thawing.

4.4.2. Runoff

As part of the validation effort of GSWP, data from many river gauging stations have been collected. This data represents the rate of river discharge measured at the station. These values can be compared against the runoff determined by each of the schemes in the basin upstream of the station. This comparison provides insight on evapotranspiration because direct observations are unattainable over such a large region and timescale. Thus, runoff agreement with river gauging observations is the best possible validation of the performance of a land surface model, which is driven by observations.

A $1° \times 1°$ global river channel network was constructed by Oki and Sud (Oki and Sud, 1998). It is called Total Runoff Integrating Pathways (TRIP); it provides lateral water movement for each grid point. Runoff generated by each of the four methods was used as input to the river routing model. Instantaneous

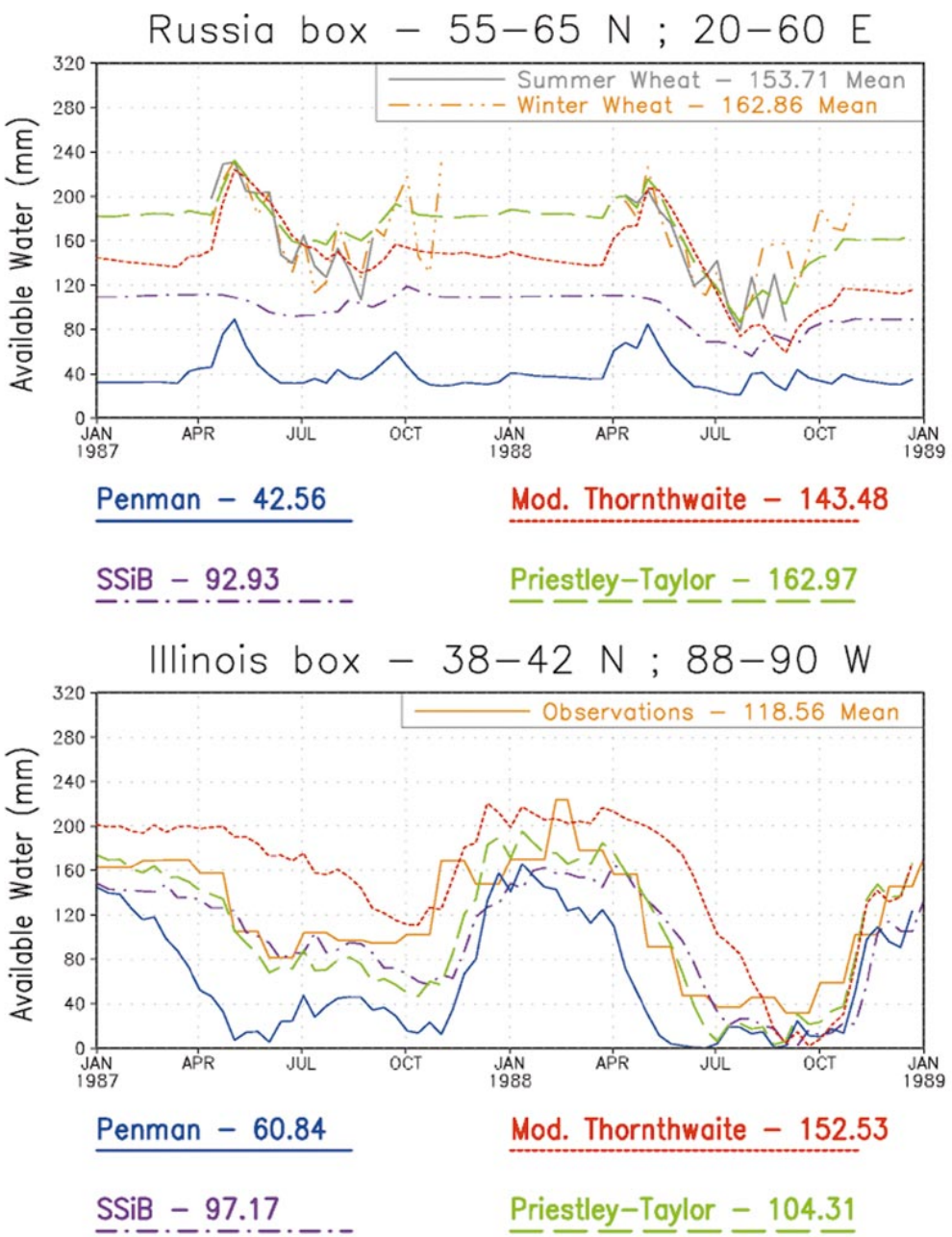

Figure 17. Time series of available soil moisture in the top meter of soil for a Russian averaging box (top) and an Illinois averaging box (bottom) for observations and all four models. Mean values are shown below each plot. Mean values for the Russia box are over only the period during which winter wheat observations are available.

point measurements made at gauging stations are then compared against the TRIP-routed runoff.

The Volga River basin is in Russia and much of the basin is contained within the Russia box of soil moisture defined earlier. Observations taken at the Volgograd power plant (44.5°N, 48.5°E) compared to TRIP-routed runoff by the four methods is shown in Figure 18. All four methods show that snowmelt and its resultant runoff is much delayed compared to observations. The 3EB methods give similar results. None of the methods produce significant runoff in late summer and winter. The SS routed runoff is excessive after the spring snowmelt, which correlates to a period of dry soil in SS as seen in the Russia box. For the Mississippi River basin (in the central United States), observations taken at Vicksburg, Mississippi (32.3°N, 63.6°W), are compared to routed runoff at this point, also in Figure 18. In this basin, SS does a very nice job, capturing both the annual cycle and having only slightly less runoff than observed. Both PT and PE produced too little runoff, while MT had too much runoff.

In all, there are dozens of river basins for which runoff observations exist for 1987–88. These observations were averaged into a 2-yr annual mean runoff and compared with the TRIP-routed runoff. Interestingly, all of the methods underestimate the annual runoff (not shown), while the MT and SS methods were noted to be better than the other two. However, Oki et al. (Oki et al., 1998) showed that nearly all land surface models perform poorly in land areas with inadequate precipitation gauge measurements. It was argued that a critical density of rain gauges is needed to provide accurate enough precipitation to drive the land surface model.

If the basins with insufficiently dense rain gauges are eliminated, and a fit is made to the remaining points of the 2-yr annual mean of observed versus modeled runoff, it is found that SS outperforms the 3EB methods as is evident from Figure 19. A slope of 1.0 would indicate a one-to-one match between the least squares fit of observations against model. Any interseasonal delay in snowmelt or runoff is smoothed out, as well as time delays due to the routing time within TRIP. The snowmelt produced by all methods is generally the same; however, a larger part of the snowmelt becomes runoff in SS because the deep soil temperature remains below freezing during the snowmelt period. The 3EB methods do not have a deep soil temperature, so the snowmelt freely infiltrates into the soil. A correction to this deficiency in SSiB is detailed in a paper Sud and Mocko (Sud and Mocko, 1998) developed from the results of this study.

Mean annual runoff over continents is listed in Table 7. The observations are taken from global water balance calculations (labeled as follows): BR75 = Baumgartner and Reichel (Baumgartner and Reichel, 1975), L73 = Lvovitch (Lvovitch, 1973), and K78 = Korzun (Korzun, 1978). For the model values, Europe and Asia are divided at 30°E, the Middle East is within Asia, tropical islands are included with the closer continent, Asia or Australia. The SS method does a more realistic job of diagnosing runoff over Africa, North America, Australia, and Asia. However, over Europe, SS runoff is too high, while for South America it is too low. Over four out of the six continents, SS does a superior job of estimating runoff as compared to the 3EB methods. As expected, PE gives the lowest runoff over all continents. This relates to high evapotranspiration and dry

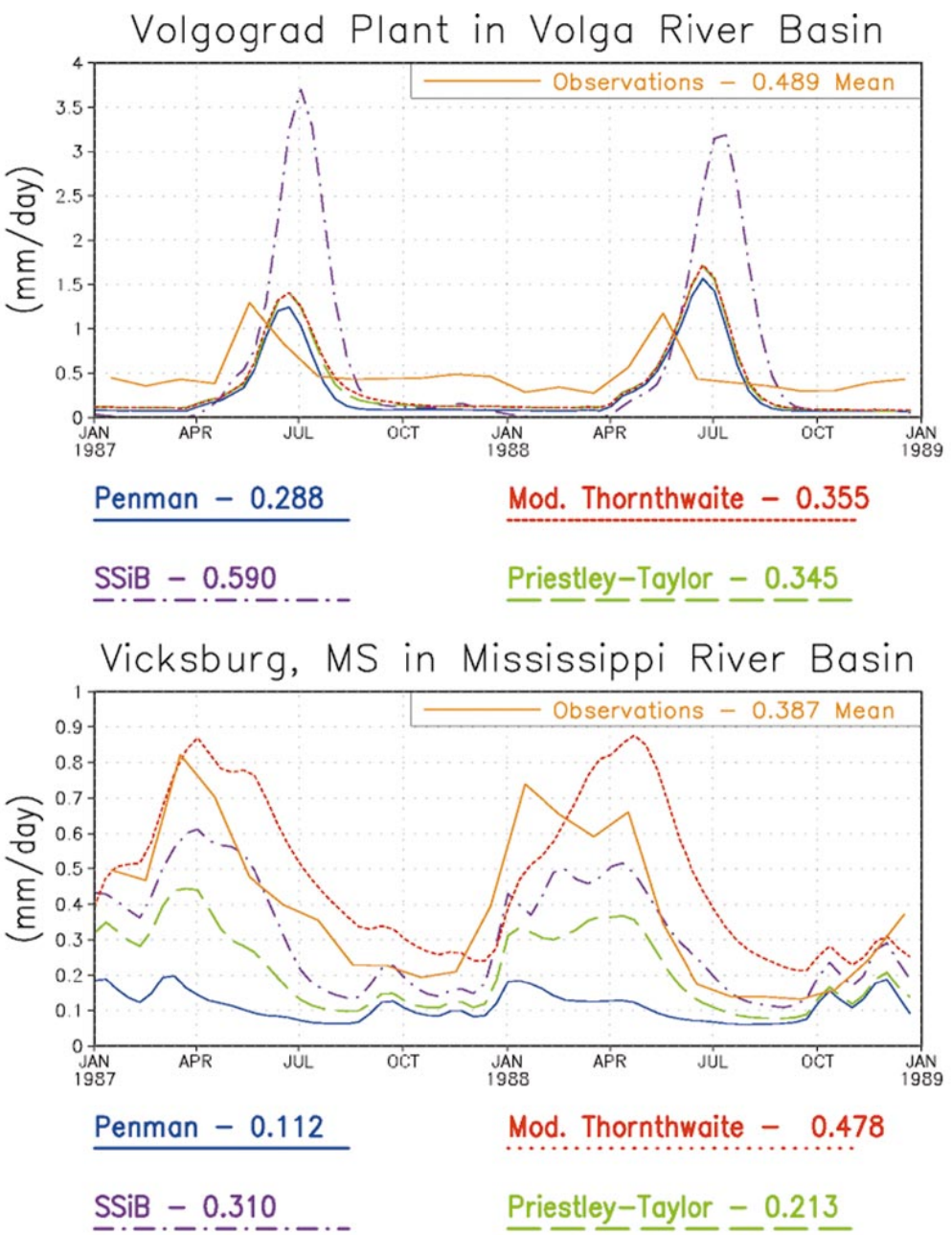

Figure 18. Surface runoff (mm day^{-1}) computed by all four models as compared to observations taken at the Volgograd plant (48.5°N, 44.5°E) in the Volga River basin (top) and at Vicksburg, MS (32.5°N, 91.5°W), in the Mississippi River basin (bottom). Mean values are shown below each plot.

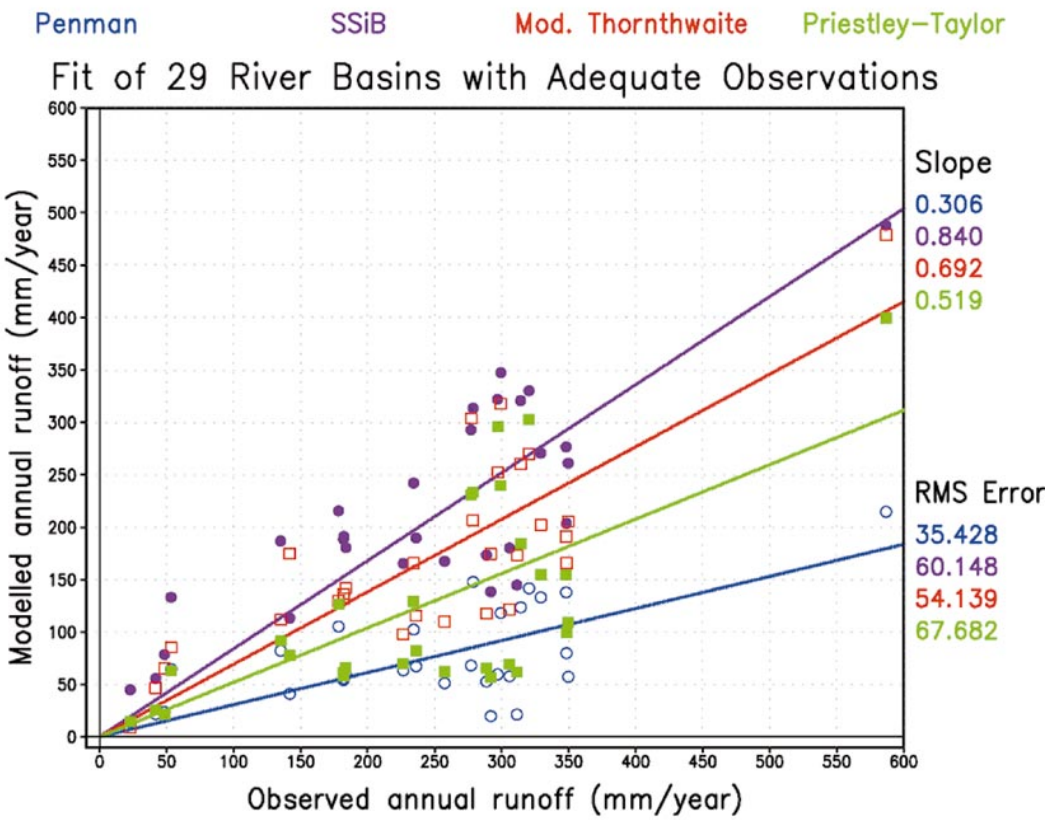

Figure 19. Fit of the runoff produced by the four methods compared to observations for river basins with a sufficient number of raingauges to provide accurate forcing precipitation. The squares and circles represent individual basins, while the lines represent a least-sqaures fit to these points, for each methods. A slope of unity would indicate a perfect fit between modeled and observed runoff. The RMSError indicates the amount of scatter of the individual basins about the fit.

soil. The PT method produces better runoff for Europe, but it is too low elsewhere. The MT method gives high runoff values, especially in Africa. In the Sahel, a very small β leads to a reduced evapotranspiration and wet soil.

5. Summary and conclusions

Four methods [three of which are energy balance methods, namely, Penman (PE), Priestley–Taylor (PT), and Mintz–Thornthwaite (MT); and a fourth method, SSiB (SS)] of estimating evapotranspiration are used to determine land surface fluxes, soil moisture, and runoff for the 2-yr integration period 1987–88, with atmospheric forcing data from ISLSCP Initiative I data.

The energy balance methods of PE and PT give higher evapotranspiration than SS, while the β calculation used in the MT method gives even lower evapo-

transpiration than SS. Model integrations using β in Mintz and Walker (Mintz and Walker, 1993) or in Xue et al. (Xue et al., 1991) for the Thornthwaite method determine evapotranspiration values as high as given by the PE and PT methods (not shown). Thus, the Mintz modification of β, though a step in the right direction, results in an overcorrection of the evapotranspiration as compared to SS. The PE and PT methods produce too much evapotranspiration in tropical forest regions. The evapotranspiration occurs at the near-potential rates. The SS method, with a biophysically governed stomatal resistance, is able to better moderate the evapotranspiration over a diurnal cycle. The MT method, by design, has a zero evapotranspiration in below-freezing regions, which leads to wet soil and high runoff.

Higher evapotranspiration leads to drier soil and less runoff, which happens in the PE and PT methods. In the MT method, the soil is much wetter and runoff is high. In comparison to runoff observations on a continental scale, SS indeed performs better than the 3EB methods. Runoff shows a strong response to evapotranspiration and, compared to other main outputs of land surface models such as fluxes and soil moisture, it is easily measurable. It is reaffirmed that runoff is an excellent measure of the performance of the land hydrology and evapotranspiration parameterization (Russell and Miller, 1990; Liston et al., 1994; Oki and Sud, 1998).

Comparisons of the simulated soil moisture to observations in Illinois show the SS model and PT method realistically produce a drier soil in the summer of 1988 and wetter soil in the summer of 1987. The MT method is too wet and the PE method is too dry. In Russia, the SS model is unable to allow snowmelt to enter the frozen soil in the early spring, which results in high surface runoff and a lack of a spring soil water recharge as observed. The other three energy balance methods, which do not calculate soil temperatures, are able to accept water from snowmelt. The PE method is again too dry, but the PT and MT methods simulate realistic soil moisture in this region.

Robock et al. (Robock et al., 1995) have previously pointed out SSiB's inability to produce realistic soil moisture in snowmelt areas. Xue et al. Xue et al., 1997 argued that inaccurate soil and vegetation parameters of the region can play a large role in mitigating the problem. This study has revealed that these problems are related to the deficiencies of the treatment of snowmelt infiltration. Consequently, a new snow model that vastly improves these deficiencies has been written for use with SSiB (detailed in Sud and Mocko, 1998).

Even though energy balance methods of evapotranspiration are unlikely to be deployed in GCMs, they are sometimes the only viable method for estimating evapotranspiration. Datasets such as provided by the ISLSCP Initiative I data are not always available and the energy balance methods do not require as detailed atmospheric forcing data and/or vegetation parameters. For scarce data situations, the energy balance methods can be considered viable methods that can yield useful information.

It should be pointed out that the 3EB methods are not similar to the bucket model. Consequently, it should not be inferred that the bucket is as poor or as good in its performance as the 3EB methods. In fact, bucket modelers have made several improvements to the bucket hydrology and it has often been found that

the bucket can match the performance of a biosphere model such as SSiB (Koster et al., 1998). However, SSiB simulations show that overall it gives superior hydrology and evapotranspiration as compared to energy balance methods via its reduction of excess evapotranspiration as verified by basin- and continental-scale runoff observations, as well as soil moisture and runoff in the continental United States.

Acknowledgments. The authors wish to thank Kenneth Bergman of NASA headquarters for supporting this research. Taikan Oki provided the gauging station and runoff observations, as well as assistance with obtaining routed runoff results. Yong-Kang Xue and Greg Walker are thanked for helpful discussions on SSiB. Alan Robock provided soil moisture observations in Russia and Illinois. Steve Hollinger provided soil moisture observations in Illinois.

Appendix. Field Capacity Derivation

The soil moisture potential equation [Sellers et al., 1986, Eq. (48)] is

$$\psi = \psi_s W^{-b}, \tag{A1}$$

which can be recast as

$$W = (\psi/\psi_s)^{-1/b}, \tag{A2}$$

where W is the soil wetness, ψ (ψ_s) is the (saturated) soil moisture potential, and b is the Clapp and Hornberger parameter.

The water flux in the soil is governed by Darcy's law (Freeze and Cherry, 1979):

$$Q = K\,[\partial\psi/\partial z + 1], \tag{A3}$$

where Q is the downward transport of water and K is the hydraulic conductivity. At the completion of drainage, $Q = 0$. Integrating the remainder of this equation yields

$$\psi = -z + c, \tag{A4}$$

where c is a constant.

If the baseflow represents soil at saturation potential, ψ_s, then the bottom boundary conditions are

$$z = D_{\text{total}}; \qquad \psi = \psi_s, \tag{A5}$$

which gives

$$c = \psi_s + D_{\text{total}}. \tag{A6}$$

Substituting c into (A4), we get

$$\psi = \psi_s + D_{\text{total}} - z. \tag{A7}$$

Substituting (A7) into (A2) and integrating over the depth of the layer, we get

$$\int_{z=D_{\text{total}}}^{z=0} W\,dz = \int_{z=D_{\text{total}}}^{z=0} [(\psi_s + D_{\text{total}} - z)/\psi_s]^{-1/b}\,dz. \tag{A8}$$

Its solution is

$$W = \text{FC}D_{\text{total}} = \frac{[(\psi_s + D_{\text{total}} - z)^{-1/b+1}]_{z=D_{\text{total}}}^{z=0}}{(-1/b + 1)\psi_s^{-1/b}}. \tag{A9}$$

Field capacity, FC, is thus

$$\text{FC} = nD\frac{(D_{\text{total}} + \psi_s)^{-1/b+1} - (\psi_s)^{-1/b+1}}{(-1/b + 1)\psi_s^{-1/b}D_{\text{total}}}, \tag{A10}$$

where n is the porosity and D is the depth, which have been multiplied to give the field capacity in terms of millimeters, instead of in terms of wetness.

References

Baumgartner, F. and E. Reichel. 1975. *The World Water Balance: Mean Annual Global, Continental and Maritime Precipitation, Evaporation and Runoff*, Ordenbourg Munich, Germany. 179–219.

Brutsaert, W. 1982. *Evaporation into the Atmosphere*, Kluwer Acad. Norwell, MA. 299–219.

Clapp, R. B. and G. M. Hornberger. 1978. Empirical equations for some soil hydraulic properties. *Water Resour. Res.*, **14**, 601–604.

Dickinson, R. E., A. Henderson-Sellers, P. J. Kennedy, and M. F. Wilson. 1986. Biosphere – Atmosphere Transfer Scheme (BATS) for the NCAR Community Climate Model. *NCAR Tech. Note TN-387 + STR*, 72 pp.

Freeze, R.A. and J.A. Cherry. 1979. *Groundwater*, Prentice-Hall. Englewood Cliffs, NJ. 604 pp.

Gates, W. L. 1992. AMIP: The Atmospheric Model Intercomparison Project. *Bull. Am. Meteorol. Soc.*, **73**, 1962–1970.

Henderson-Sellers, A., Z.-L. Yang, and R. E. Dickinson. 1993. The Project for Intercomparison of Land-surface Parameterization Schemes. *Bull. Am. Meteorol. Soc.*, **74**, 1335–1349.

Henderson-Sellers, A., A. J. Pitman, P. K. Love, P. Irannejad, and T. H. Chen. 1995. The Project for Intercomparison of Land-surface Parameterization Schemes (PILPS): Phases 2 and 3. *Bull. Am. Meteorol. Soc.*, **76**, 489–503.

Hollinger, S. E. and S. A. Isard. 1994. A soil moisture climatology of Illinois. *J. Clim.*, **7**, 822–833.

International GEWEX Project Office. 1995. Global Soil Wetness Project, version 1.0. 47 pp. [Available from International GEWEX Project Office, 1100 Wayne Avenue, Suite 1210, Silver Spring, MD 20910.].

Jensen, L. 1973. *Consumption Use of Water and Irrigation Water Requirements*, Amer. Soc. Civil Engineers, Reston, VA. 215 pp.

Korzun, V. I. 1978. *World Water Balance and Water Resources of the Earth*, Vol. 25, Studies and Reports in Hydrology, UNESCO, Geneva, Switzerland. 587 pp.

Koster, R. D., T. Oki, and M. J. Saurez. 1998. Assessing success in the offline validation of land surface models. *J. Meteorol. Soc. Jpn.*, submitted.

Lau, K.-M., J. H. Kim, and Y. C. Sud. 1996. Intercomparison of hydrologic processes in AMIP GCMs. *Bull. Am. Meteorol. Soc.*, **77**, 2209–2227.

Liston, G. E., Y. C. Sud, and G. K. Walker. 1993. Design of a global soil moisture initialization procedure for the simple biosphere model. *NASA Tech. Memo. 104590*, 130 pp. [NTIS N94-10940/2INZ.].

Liston, G. E., Y. C. Sud, and E. F. Wood. 1994. Evaluating GCM land surface hydrology parameterizations by computing river discharges using a runoff routing model: Application to the Mississippi Basin. *J. Appl. Meteorol.,* **33**, 394–405.

Lvovitch, M. I. 1973. The global water balance. *Trans. AGU,* **54**, 28–42.

Mahrt, L. and M. Ek. 1984. The influence of atmospheric stability on potential evaporation. *J. Clim. Appl. Meteorol.,* **23**, 222–234.

Manabe, S. 1969. The atmospheric circulation and the hydrology of the earth's surface. *Mon. Weather Rev.,* **97**, 739–774.

Meeson, B. W., F. E. Corprew, J. M. P. McManus, D. M. Myers, J. W. Closs, K.-J. Sun, D. J. Sunday, and P. J. Sellers. 1995. *ISLSCP Initiative I —Global Data Sets for Land–Atmosphere Models, 1987–1988,* NASA, published on CD-ROM (USA_NASA_GDAAC_ISLSCP_001-USA_NASA_GDAAC_ISLSCP_005).

Milly, P. C. D. 1992. Potential evaporation and soil moisture in general circulation models. *J. Clim.,* **5**, 209–226.

Mintz, Y. and Y. Serafini. 1984. Global fields of monthly normal soil moisture as derived from observed precipitation and estimated potential evapotranspiration. Part V. *NASA Grant NAS5-26,* 182 pp. [Available from Dept. of Meteorology, University of Maryland, College Park, MD 20742.].

Mintz, Y. and Y. Serafini. 1992. A global monthly climatology of soil moisture and water balance. *Clim. Dyn.,* **8**, 13–27.

Mintz, Y. and G. K. Walker. 1993. Global fields of soil moisture and land surface evapotranspiration derived from observed precipitation and surface air temperature. *J. Appl. Meteorol.,* **32**, 1305–1334.

Oki, T. and Y. C. Sud. 1998. Design of Total Runoff Integrating Pathways (TRIP)—A global river channel network. *Earth Interactions,* **2**, 2-001.

Oki, T., T. Nishimura, and P. Dirmeyer. 1998. Validating land surface models by runoff in major river basins of the globe using Total Runoff Integrating Pathways (TRIP). *J. Meteorol. Soc. Jpn.,* submitted.

Pan, H.-L. 1990. A simple parameterization scheme of evapotranspiration over land for the NMC medium-range forecast model. *Mon. Weather Rev.,* **118**, 2500–2512.

Penman, H. L. 1948. Natural evaporation from open water, bare soil, and grass. *Proc. Roy. Soc. London Ser. A.,* **193**, 120–145.

Priestley, C. H. B. and R. J. Taylor. 1972. On the assessment of surface heat flux and evaporation using large-scale parameters. *Mon. Weather Rev.,* **100**, 81–92.

Robock, A., K. Ya. Vinnikov, C. A. Schlosser, N. A. Speranskaya, and Y. Xue. 1995. Use of midlatitude soil moisture and meteorological observations to validate soil moisture simulations with biosphere and bucket models. *J. Clim.,* **8**, 15–35.

Russell, G. L. and J. R. Miller. 1990. Global river runoff calculated from a global atmospheric general circulation model. *J. Hydrol.,* **117**, 241–254.

Sato, N., P. J. Sellers, D. A. Randall, E. K. Schneider, J. Shukla, J. L. Kinter III, Y.-T. Hou, and E. Albertazzi. 1989. Effects of implementing the Simple Biosphere Model in a general circulation model. *J. Atmos. Sci.,* **46**, 2757–2782.

Sellers, P. J. 1985. Canopy reflectance, photosynthesis and transpiration. *Int. J. Remote Sens.,* **6**, 1335–1372.

Sellers, P. J., Y. Mintz, Y. C. Sud, and A. Dalcher. 1986. A simple biosphere model (SiB) for use within general circulation models. *J. Atmos. Sci.,* **43**, 505–531.

Sellers, P. J., S. O. Los, C. J. Tucker, C. O. Justice, D. A. Dazlich, G. J. Collatz, and D. A. Randall. 1996a. A revised land surface parameterization (SiB2) for atmospheric GCMs. Part II: The generation of global fields of terrestrial biophysical parameters from satellite data. *J. Clim.,* **9**, 706–737.

Sellers, P. J. and Coauthors. 1996b. The ISLSCP Initative I global datasets: Surface boundary conditions and atmospheric forcings for land-atmosphere studies. *Bull. Am. Meteorol. Soc.*, **77**, 1987–2005.

Sellers, P. J. and Coauthors. 1996c. A revised land surface parameterization (SiB2) for atmospheric GCMs. Part I: Model formulation. *J. Clim.*, **9**, 676–705.

Serafini, Y. V. and Y. C. Sud. 1987. The time scale of the soil hydrology using a simple water budget model. *J. Climatol.*, **7**, 585–591.

Sud, Y. C. and M. J. Fennessy. 1982. An observational-data based evapotranspiration function for general circulation models. *Atmos.–Ocean.*, **20**, 301–316.

Sud, Y. C. and W. E. Smith. 1984. Ensemble formulation of surface fluxes and improvement in evapotranspiration and cloud parameterization in a GCM. *Boundary Layer Meteorol.*, **29**, 185–210.

Sud, Y. C. and D. M. Mocko. 1998. Development and evaluation of a new snow-physics model to complement SSiB (Part I). *J. Meteorol. Soc. Jpn.*, in press.

Sud, Y. C., P. J. Sellers, Y. Mintz, M. D. Chou, G. K. Walker, and W. E. Smith. 1990. Influence of the biosphere on the global circulation and hydrologic cycle–a GCM simulation experiment. *Agric. For. Meteorol.*, **52**, 133–180.

Thornthwaite, C. W. 1948. An approach toward a rational classification of climate. *Geogr. Rev.*, **38**, 55–94.

Tucker, C. J., J. R. G. Townshend, and T. E. Goff. 1985. African land-cover classification using satellite data. *Science.*, **227**, 369–375.

Vinnikov, K. Y. and I. B. Yeserkepova. 1991. Soil moisture: Empirical data and model results. *J. Clim.*, **4**, 66–79.

Xue, Y., P. J. Sellers, J. L. Kinter, and J. Shukla. 1991. A simplified biosphere model for global climate studies. *J. Clim.*, **4**, 345–364.

Xue, Y., P. J. Sellers, F. J. Zeng, and C. A. Schlosser. 1997. Comments on ''Use of midlatitude soil moisture and meteorological observations to validate soil moisture simulations with biosphere and bucket models''. *J. Clim.*, **10**, 374–376.

Table 1. Description of soil types used in the models and values for porosity, matric potential at saturation (m), saturated hydraulic conductivity (m s^{-1}), and Clapp and Hornberger parameter. Soil type 6 is permanent ice—these points were not included in this study.

Soil type	Description	n	ψ_s	K_s	b
1	coarse	0.421	0.0363	1.41×10^{-5}	4.26
2	medium/coarse	0.434	0.1413	5.23×10^{-6}	4.74
3	medium	0.439	0.3548	3.38×10^{-6}	5.25
4	fine/medium	0.404	0.1349	4.45×10^{-6}	6.77
5	fine	0.465	0.2630	2.45×10^{-6}	8.17
7	organic	0.439	0.3548	3.38×10^{-6}	5.25

Table 2. Two-year global area average for energy balance terms.

All units (W m^{-2})	PE	PT	MT	SS
Evapotranspiration	49.4	45.2	30.3	37.5
Sensible heat	41.5	45.8	60.6	39.4
Ground heat	0.02	0.02	0.02	1.7
Snowmelt heat	0.6	0.6	0.6	0.7
SW down	187.7	187.7	187.7	187.7
SW up	36.6	36.6	36.6	37.0
LW down	322.6	322.6	322.6	322.6
LW up	382.2	382.2	382.2	393.9
Net SW	151.1	151.1	151.1	150.7
Net LW	−59.5	−59.5	−59.6	−71.3
R_{net}	91.5	91.5	91.5	79.4

Table 3. Forcing data divided by vegetation type.

Vegetation type	P_t (mm day^{-1})	T_A (°C)	$S_\downarrow$ (W m^{-2})	$L_\downarrow$ (W m^{-2})
1	5.50	23.1	205.0	406.5
2	2.43	15.1	194.5	338.3
3	2.30	7.6	152.2	300.9
4	1.44	−3.3	120.6	253.8
5	1.20	−7.6	115.8	235.5
6	3.35	19.6	207.3	366.8
7	1.63	13.0	194.0	319.6
9	0.69	16.6	222.4	322.7
10	0.89	11.6	99.6	219.8
11	0.25	19.3	239.6	335.9

Table 4. Evapotranspiration (W m^{-2}) for all four models—divided by vegetation type.

Vegetation type	PE	PT	MT	SS
1	136.5	116.8	88.9	99.7
2	63.1	59.9	39.9	49.7
3	61.1	52.1	41.3	45.2
4	34.9	29.5	24.0	20.5
5	28.0	25.6	24.5	18.8
6	78.2	75.1	47.1	60.3
7	39.7	38.4	22.2	33.5
9	19.1	19.0	7.7	17.7
10	17.4	14.2	10.5	7.3
11	6.9	6.8	2.3	6.2

Table 5. Available water (mm) for all four models—divided by vegetation type.

Vegetation type	PE	PT	MT	SS
1	93.0	153.8	179.3	126.8
2	41.5	80.4	132.3	79.1
3	43.4	124.6	143.6	88.8
4	26.9	103.2	108.7	60.1
5	11.2	71.5	40.0	17.1
6	68.6	83.6	137.6	119.1
7	38.3	49.6	131.5	40.5
9	8.2	12.6	156.5	0.4
10	77.8	110.7	105.7	100.4
11	1.8	4.1	83.5	9.8

Table 6. Total runoff (mm day^{-1}) for all four models—divided by vegetation type.

Vegetation type	PE	PT	MT	SS
1	0.74	1.38	2.31	1.98
2	0.26	0.39	1.04	0.73
3	0.19	0.51	0.88	0.76
4	0.22	0.42	0.62	0.74
5	0.23	0.30	0.36	0.55
6	0.64	0.74	1.66	1.25
7	0.27	0.31	0.86	0.48
9	0.03	0.03	0.41	0.08
10	0.27	0.38	0.52	0.63
11	0.01	0.01	0.16	0.04

Table 7. Mean annual continental-scale total runnoff (mm yr^{-1}) computed by all four models as compared to observations.

Continent	BR75	L73	K78	PE	PT	MT	SS
Asia	260	281	300	121	163	316	261
Europe	255	273	273	129	294	321	328
Africa	113	140	153	54	56	267	135
North America	223	258	315	84	137	262	228
South America	611	578	678	223	346	629	511
Australia	267	222	278	113	147	394	238